

We are IntechOpen, the world's leading publisher of Open Access books Built by scientists, for scientists

6,900

Open access books available

186,000

International authors and editors

200M

Downloads

Our authors are among the

154

Countries delivered to

TOP 1%

most cited scientists

12.2%

Contributors from top 500 universities



WEB OF SCIENCE™

Selection of our books indexed in the Book Citation Index
in Web of Science™ Core Collection (BKCI)

Interested in publishing with us?
Contact book.department@intechopen.com

Numbers displayed above are based on latest data collected.
For more information visit www.intechopen.com



Single-Phase Heat Transfer and Fluid Flow Phenomena of Microchannel Heat Exchangers

Thanhtrung Dang¹, Jyh-tong Teng², Jiann-cherng Chu², Tingting Xu³,
Suyi Huang³, Shiping Jin³ and Jieqing Zheng⁴

¹*Department of Heat and Refrigeration Technology, Hochiminh City University of Technical Education, Hochiminh City,*

²*Department of Mechanical Engineering, Chung Yuan Christian University, Chung-Li,*

³*School of Energy and Power Engineering, Huazhong University of Science and Technology, Wuhan,*

⁴*College of Mechanical Engineering, Jimei University, Xiamen, Fujian,*

¹*Vietnam*

²*Taiwan*

^{3,4}*P. R. China*

1. Introduction

In recent years, microfabrication technologies have been utilized in the fields of process engineering using microchannel devices as heat exchangers. The microchannel heat transfer means is of importance to the areas of small and confined spaces, high heat flux devices for cooling electronic components, or other cooling applications in thermal and chemical engineering. Increasing the heat transfer rate and decreasing characteristic dimension of a heat exchanger are key design requirements, and a micro heat exchanger satisfies these needs.

A review of micro heat exchanger related issues such as flow behaviors, fabrication methods, and practical applications was done by Bowman and Maynes [1]. The review firstly introduced the experimental and numerical investigations of channel flow. Subsequently, Friction and heat transfer measurements of gas flow and liquid flow were discussed in the paper. The paper indicated that the transition Reynolds number is a function of surface roughness and channel geometry. Moreover, in the paper, the heat exchanger designs - including their comparison and optimization - were also reviewed. Furthermore, several fabrication methods including micromachining, chemical etching, laser machining, electroplating, and lamination, were discussed.

Review of the experimental results concerning single-phase convective heat transfer in microchannels was presented by Morini [2], with additional review of the results obtained for friction factor, laminar-to-turbulent transition, and Nusselt number in channels having hydraulic diameters less than 1 mm. Dang [3] and Dang et al. [4] presented the fluid flow

and heat transfer characteristics for rectangular-shaped microchannel heat exchangers, both numerically and experimentally. Effects of flow arrangement on the performance index (expressed as the ratio of the heat transfer rate to the pressure drop) of a microchannel heat exchanger were evaluated. In addition, influences of configurations on the performance index of microchannel heat exchangers were presented.

Brandner et al. [5] described microstructure heat exchangers and their applications in laboratory and industry. In their paper, several micro heat exchangers were introduced, including polymer microchannel heat exchanger with aluminum separation foil, electrically powered lab-scale microchannel evaporator, ceramic counter-flow microstructure heat exchanger, etc. An analysis of effectiveness and pressure drop in micro cross-flow heat exchanger was presented by Kang and Tseng [6]. For each effectiveness, the heat transfer rate and pressure drop as a function of average temperature were obtained. The results indicated that pressure drop was reduced with a rising average temperature. Using silicon or copper as the materials for the microchannel heat exchangers, the difference in heat transfer rates between these two types of heat exchangers was found to be minimal. This was due to the fact that the substrate thicknesses between the hot and the cold channels were very thin; as a result, their thermal conductivity resistances were very small. Henning et al. [7] made three devices – the “standard” channel device with straight layout and a hydraulic diameter of 153 μm , the “short” channel with straight layout and a hydraulic diameter of 149 μm , and the “wavy” channel with wavy layout and a hydraulic diameter of 125 μm . Their experimental results indicated that the standard channel device was the best choice for heating at moderate and high flow rates.

The crossflow microstructure heat exchanger made of stainless steel W316L was studied by Brandner [8]. It was observed that heat transfer in a microstructure heat exchanger was enhanced by using staggered microcolumn array heat exchangers which were designed to operate in the transition or turbulent flow regime. Results obtained from experiments and from modeling of an integrated preferential oxidation-heat exchanger (ProxHeatex) microdevice were presented by Delsman et al. [9]. The ProxHeatex consisted of two heat exchangers and a cooled reactor, as shown in Fig. 1. Those researchers also improved a new version of a ProxHeatex from an earlier prototype [10]. Heat recovery efficiency of the ProxHeatex device was found to be a function of the reformatted gas flow rate. The overall heat recovery of the device varies between 73% and 95%, with the higher values corresponding to higher flow rates and higher oxygen excess.

Shen and Gau [11] presented a paper dealing with design and fabrication of sensors and heaters for the study of micro-jet impingement cooling. The local Nusselt number distribution along the wall, Nu_x , was found to be a function of Z/B ratio, where Z is nozzle-to-wall distance and B is the slot width. A heat exchanger for power electronic components was studied by Gillot et al. [12]. The prototype was composed of four elementary modules. Each module was composed of two IGBT (Insulated Gate Bipolar Transistor) chips directly brazed onto a piece of copper where rectangular channels were machined. The thermal resistance of the chips was calculated using 3D finite element simulation tool (FLUX 3D). Numerical and experimental values of the metal temperature at five testing locations were in good agreement, with the maximum percentage error being 1.7%. The pressure drop observed to be increased with a rising flow rate. The heat spread effect was observed to be a function of the heat transfer coefficient.

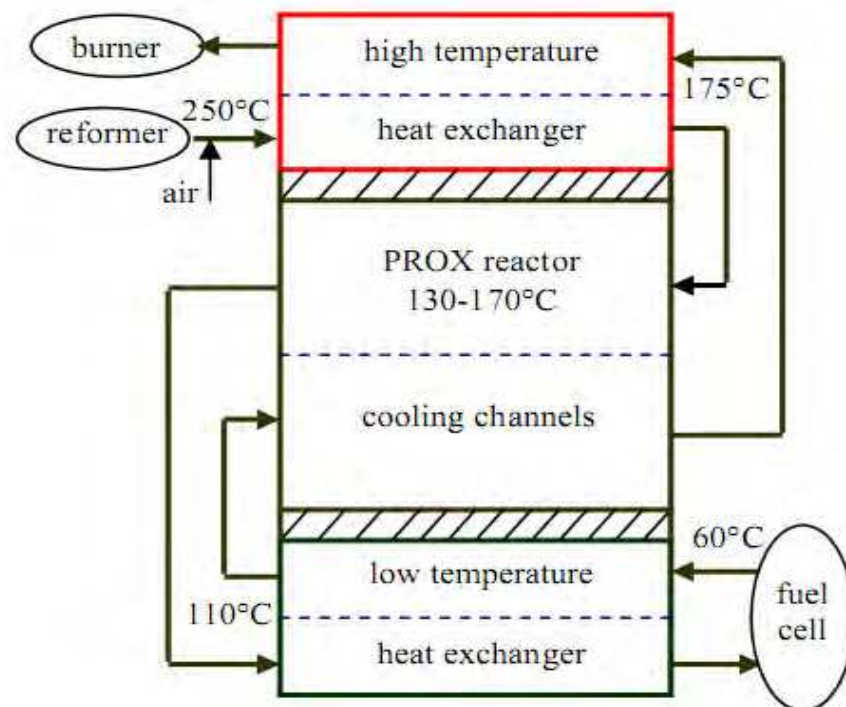


Fig. 1. Schematic of the integrated preferential oxidation-heat exchanger [3,4,9,10].

Ceramic microstructure devices in the forms of counter-flow and cross-flow microchannel heat exchangers were manufactured by Alm et al. [13] and used in thermal and chemical process engineering. The peak experimental heat transfer coefficient for the cross-flow heat exchanger was observed to reach $22 \text{ kW}/(\text{m}^2\text{K})$. Hallmark et al. [14] presented an experimental investigation on the heat transfer response of plastic microcapillary films (MCF). Thermal power removed by the MCF heat exchanger was shown to be a function of input electrical power for an increasing flow rate of the MCF. Jiang et al. [15] investigated fluid flow and forced convection heat transfer in microchannel heat exchanger (MCHE). The transition from laminar to turbulent flow in the microchannel heat exchanger was observed to occur at $Re \approx 600$. A new method of fabrication of heat transfer surfaces with micro-structured profile was presented by Schulz et al. [16]. By the ion track etching combined with metal electro-plating method, arrays of copper whiskers with high aspect ratio were produced on surfaces of heat transfer tubes. At the same temperature, the structured tube had higher heat flux or heat transfer coefficient value than that of the smooth one. Lee et al. [17] studied a polymer type micro-heat exchanger applicable to 272 BGA multi-chip module (MCM) and selected polydimethylsiloxane (PDMS) as the package material. The design was evaluated numerically using the Fluent CFD simulation tool. Results obtained from both the experiment and the simulation for each fabricated heat exchanger were compared; difference of temperature distribution in chip was less than 2°C . Surface temperature of the chip was found to be a function of pressure drop, the temperature decreased with a rising of the pressure drop for all the conditions being tested.

Wei [18] fabricated a stacked microchannel heat sink using microfabrication techniques. Experiments were conducted to study the thermal performance of stacked microchannel structure, and overall thermal resistance was determined to be less than 0.1 K/W for both counter-flow and parallel-flow configurations. In the study, the numerical simulations were

| References | Material/ Shape | Working fluid | Flow rate | Heat transfer | Pressure drop | Comments |
|----------------|-----------------------------------|-----------------------|---|---|--|--|
| Brandner [5] | Polymer | Water | m: 10-400 kg/h | q: 0.2-1.1 W/cm ² | 0-0.4 MPa | |
| Kang [6] | Silicon/ Rect Copper/ Rect | Water Water | m: 0.0643-0.07 kg/s m: 0.1746-0.0026 kg/s m: 0.0663-0.724 kg/s m: 0.1803-0.0027 kg/s | Q: 2,690-2,925 W Q: 500-7,300 W Q: 2,780-3,030 W Q: 500-7,500 W | 0.16-0.28 MPa (Hot side) 0.22-0.44 MPa (Cold side) 10-400 kPa (Hot side) 10-900 kPa (Cold side) | Given the same effectiveness Given the same temperature Given the same effectiveness Given the same temperature |
| Henning [7] | Metal | Water | m: 64 kg/h | Q: 3,000 W | None | Electrical power up to 3 kW with effectiveness ~ 0.95 |
| Brandner [8] | Stainless steel/ Rect | Water | m: 0-400 kg/h m: 0-300 kg/h | Q: 0-8,500 W Q: 0-12,000 W | 0-6.2x10 ⁵ Pa None | For hydraulic diameter of 70 μm For staggered microcolumns |
| Delsman [9,10] | Stainless steel/ Rect | Methanol, water | V: 2.5-6 SLM | Heat recovery efficiency of the ProHeatex: 73-95% | | |
| Shen [11] | Silicon/ Rect | Air | None | $\overline{Nu} = 0.045 Re \left(\frac{Z}{L} \right)^{0.4}$ $\overline{Nu} = 0.052 Re \left(\frac{Z}{L} \right)^{-0.5}$ | None None | For the case before jet breakdown For the case after jet breakdown |
| Gillot [12] | Copper/ Rect | Water with 40% glycol | V: 130-280 ml/s | R: 100-110 K/kW | 50-200 kPa | |
| Alm [13] | Ceramic | Water | m: 10-140 kg/h | h: 7-22 kW/m ² K (For crossflow HE) | 20-450 kPa (For counterflow HE) | |
| Hallmark [14] | Plastic | Water | V: 30 or 60 or 120 mL/min | h: 125-230 W/m ² K | None | |
| Jiang [15] | Copper/ Rect | Water | m: 0.0093-0.34 kg/s | K _v : 11-38.5 MW/m ³ K | 3.3-90 kPa | |
| Schulz [16] | Copper/ tube | Water | V: 4 L/m | q: 1,000-17,000 W/m ² | None | Overheat from 4-16 °C |
| Lee [17] | PDMS/ Rect | Water | None | Q: 0-14 W | 0-10 kPa | The top chip's temperature was 125 °C |

| References | Material/Shape | Working fluid | Flow rate | Heat transfer | Pressure drop | Comments |
|--------------|---------------------|---------------|--|--|---------------|---|
| Wei [18] | Silicon/Rect | Water | V: 1.4×10^{-6} - 5.8×10^{-6} m ³ /s | R: 0.24×10^{-4} - 0.12×10^{-4} °Cm ² /W | p = f(V) | for several channels |
| Hasan [19] | Silicon | Water | Re = 50 | $\varepsilon = f(\text{Kr})$ | 7.8 kPa | For rectangular channel |
| Dang [21-31] | Silicon/Trapezoidal | Water | m: 0.0579-0.1158 g/s | q: 12 - 13.6 W/cm ² | None | |
| | Aluminum/Rect | Water | m: 0.1859-0.3625 g/s | q: 6.5 - 8.2 W/cm ² | 500-1400 Pa | With the mass flow rate of the hot side of 0.1667 g/s |
| | Aluminum/Rect | Water | m: 0.2043-0.401g/s | q: 14.3 - 17.8 W/cm ² ξ : 13.9-21.7 W/kPa | | With the mass flow rate of the hot side of 0.2321 g/s |

(Note: Rect- Rectangular, Q-heat transfer rate, q-heat flux, R-thermal resistance, h-heat transfer coefficient, K_v-volumetric heat transfer coefficient, \overline{Nu} -average Nusselt number, SLM-standard liter per minute, m-mass flow rate, V-volume flow rate, PDMS- polydimethylsiloxane, Z- nozzle-to-wall distance, L- distance from nozzle to the breakdown point of the jet, HE-heat exchanger), Kr-thermal conductivity ratio, and ξ - performance index)

Table 1. Summary of the microchannel heat exchangers with single phase flow [3,4].

also done by using Fluent CFD package. Hasan et al. [19] evaluated the effect of the size and shape of channels for a counter-flow microchannel heat exchanger by using Fluent CFD numerical simulation. The effect of various channels showed that the circular shape achieved the best overall performance, with the second being the square channels. Results obtained from the numerical analyses and the experimental data of [18, 19] were in good agreement with the maximum error being 5.1% and the maximum difference in wall temperature being 1.7 K. Ameel et al. [20] presented an overview of the miniaturization technologies and their applications to energy systems. Based on the MEMS (microelectromechanical systems) technologies, the processes (including silicon-based micromachining, deep X-ray lithography, and the micro mechanical machining) were discussed in the context of applications to fluid flow, heat transfer, and energy systems.

A study on the simulations of a trapezoidal shaped micro heat exchanger was presented by Dang et al. [21]. Using the geometric dimensions and the flow condition associated with this micro heat exchanger, a heat flux of 13.6 W/cm² was determined by the numerical method. The effects of flow arrangement on the heat transfer behaviors of a microchannel heat exchanger were presented by Dang et al. [22-25]. For all cases done in these studies, the heat flux obtained from the counter-flow arrangement was observed to be always higher than that obtained from the parallel-flow: the value obtained from the counter-flow was evaluated to be 1.1 to 1.2 times of that obtained from the parallel-flow. The authors also presented an experimental study of the effects of gravity on the behaviors of heat transfer and pressure drop of a microchannel heat exchanger. The results showed that for microchannel heat exchangers, the influence of gravity on the pressure drop and heat transfer behaviors was negligibly small [26, 27].

Dang and Teng [28, 29] studied the effects of the configuration (such as substrate thickness, cross-sectional area, and inlet/outlet location) on the behaviors of heat transfer and fluid flow of the microchannel heat exchangers. It was found that the actual heat transfer rate was observed to vary insignificantly with the substrate thickness in the range from 1.2 to 2 mm. Moreover, a comparison of the pressure drop and heat transfer behaviors between the microchannel and minichannel heat exchangers was done by Dang et al. [30]. Furthermore, numerical simulations of the microchannel heat exchangers using solver with the capability of dealing with steady-state and time-dependent conditions were carried out [31]. Numerical studies of the behaviors of the microchannel heat exchangers with 3D single-phase fluid flow and heat transfer in [22-26, 28-31] were done by using the COMSOL Multiphysics software, version 3.5. The algorithm of this software was based on the finite element method. The results obtained from the simulation were in good agreement with those obtained from the experiments, with the maximum percentage error being less than 9%.

To summarize, Table 1 listed the heat transfer and fluid flow behaviors for single phase microchannel heat exchangers [3, 4]. The heat exchangers were manufactured by different materials with a variety of shapes. Water was the most frequently used working fluid. The heat transfer coefficient and pressure drop were observed to be functions of the mass flow rate. The staggered microcolumn array and the micro-structured surface were found to enhance heat transfer rate in the micro heat exchangers. Because that the substrate thickness (between the hot and the cold channels) of micro heat exchangers was very thin, so the differences between the heat transfer rates obtained from these heat exchangers were negligibly small for several materials used in the studies.

From the above literatures, it is important to better understand the behaviors of heat transfer and pressure drop of the fluid through the microchannel heat exchangers in order to improve their design and optimize their performance. For the present study, single phase heat transfer and fluid flow phenomena obtained from experiments and numerical simulations for rectangular-shaped microchannel heat exchangers were investigated. In the following sections, five heat exchangers with different geometrical configurations will be discussed.

2. Experimental method

2.1 Experimental setup

Three major parts are used in the experimental system: the test section (the microchannel heat exchangers), syringe system, and overall testing loop, as shown in Fig. 2, with four microchannel heat exchangers being tested. The heat transfer process of these devices is carried out between two liquids which are hot water and cold water; the hot and cold fluids are flowing in the opposite directions.

Fig. 3 shows the dimensions of the test sections. The material used for the substrate of heat exchangers is aluminum, with thermal conductivity of 237 W/(mK), density of 2,700 kg/m³, and specific heat at constant pressure of 904 J/(kgK). For each microchannel heat exchanger, the top side for the hot water has 10 microchannels and the bottom side for the cold water also has 10 microchannels. The length of each microchannel is 32 mm. Microchannels have rectangular cross-section with the width and the depth being W_c and D_c , respectively.

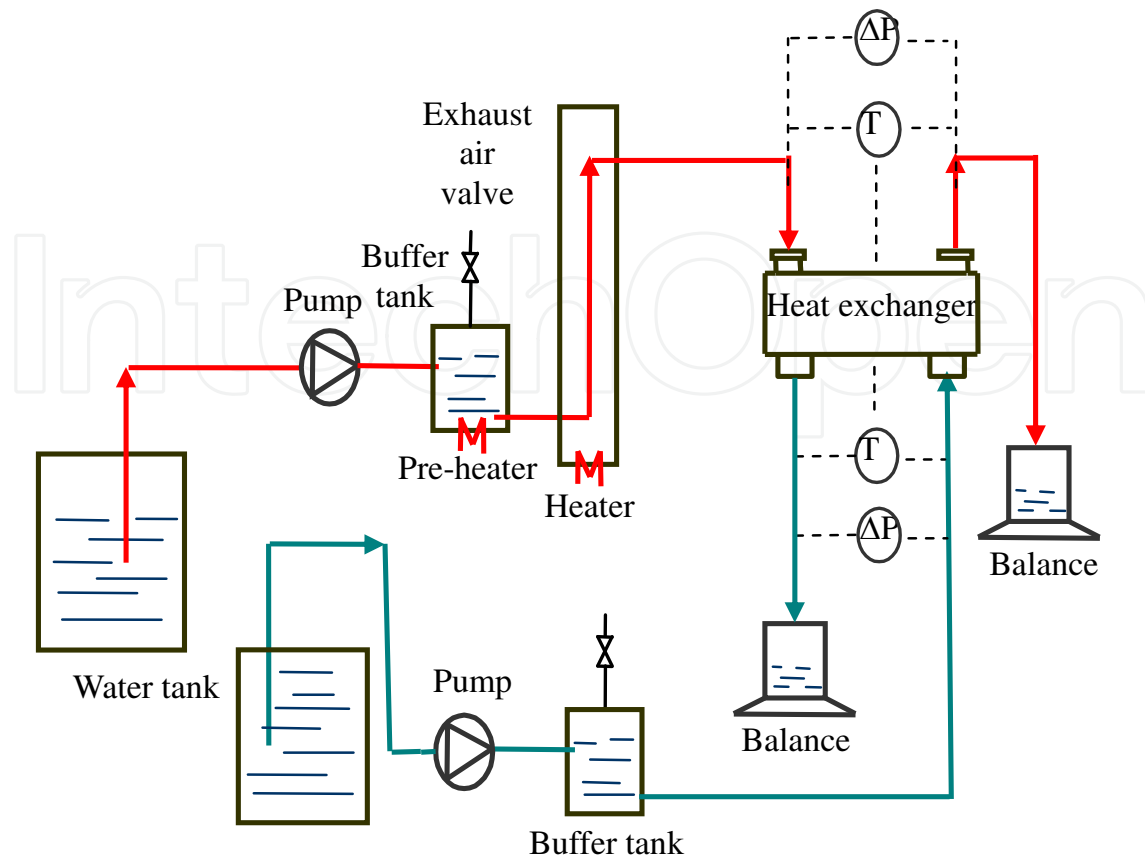
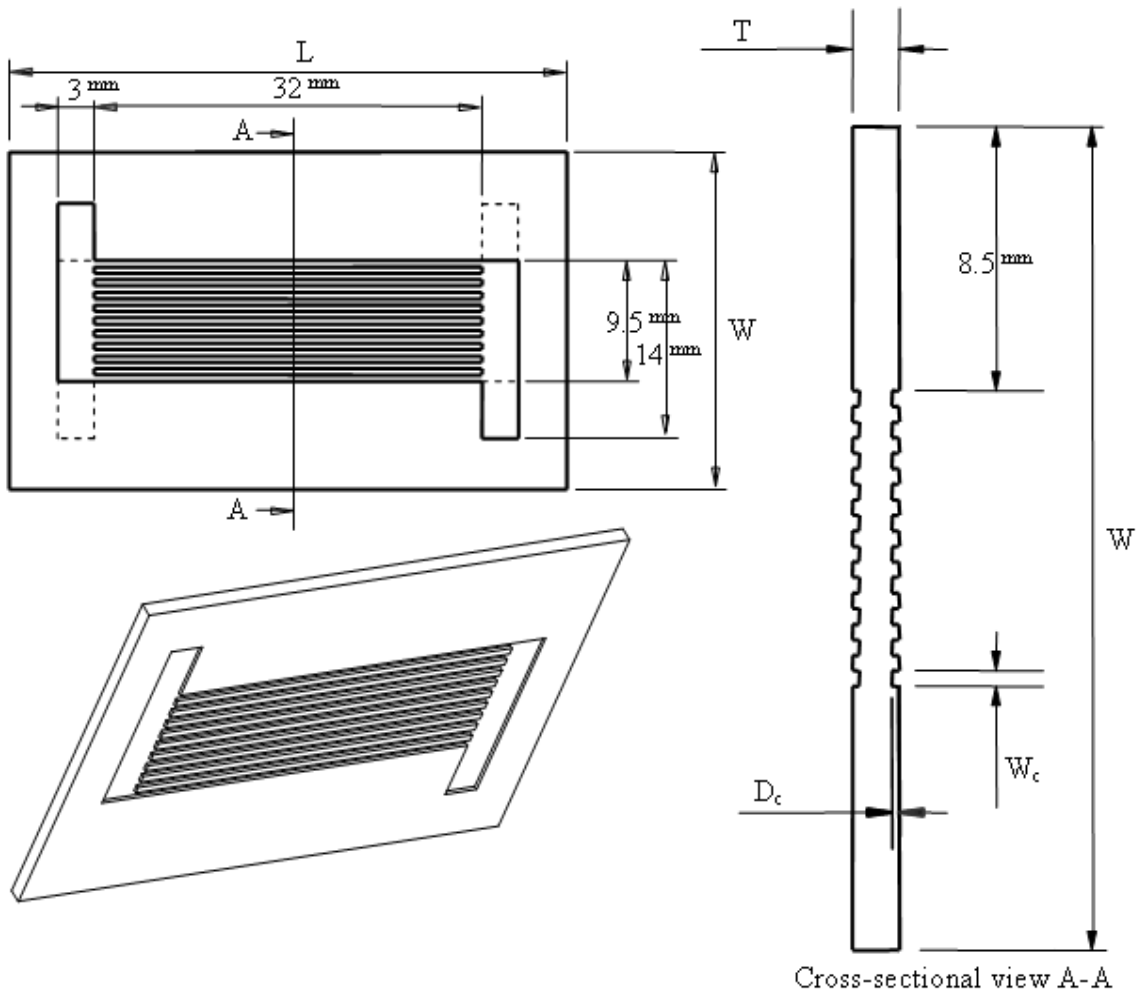


Fig. 2. Schematic of the test loop for the heat exchangers [3, 22-31].

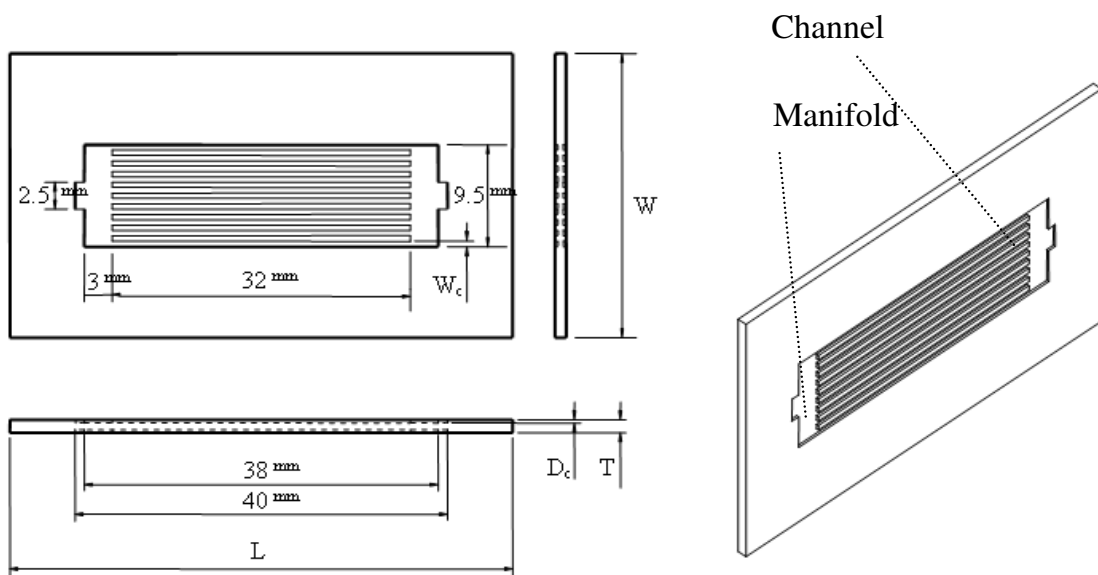
In a microchannel heat exchanger, all channels are connected by manifolds for the inlet and outlet of hot water and for those of cold water, respectively. The manifolds of the heat exchangers are of the same cross-sections: having a rectangular shape with a width of 3 mm and a depth of 300 μm . Figs. 3a and 3b show the dimensions of the S-types and I-type, respectively, with three S-types and one I-type being designed and manufactured and their dimensions listed in Table 2. Fig. 4 shows the photos of the microchannel heat exchangers with S-type and I-type manifolds. These test sections were manufactured by precision micromachining [20]. Each inlet hole or outlet hole of the heat exchangers has a cross-sectional area of 9 mm². The four sides of the heat exchanger were thermally insulated by the glass wool with a thickness of 5 mm. To seal the microchannels, two layers of PMMA (polymethyl methacrylate) were bonded on the top and bottom sides of the substrate by UV (ultraviolet) light process, as shown in Fig. 4. The physical properties of the PMMA and the glass wool are listed in Table 3 [32].

| No. | Type | Dimensions of the substrate (mm) | | | Dimensions of the channel (μm) | |
|-----|------------------------|----------------------------------|------|-----|---|-------|
| | | L | W | T | W_c | D_c |
| T1 | S- Type (Microchannel) | 46 | 26.5 | 1.2 | 500 | 300 |
| T2 | S- Type (Microchannel) | 46 | 26.5 | 2 | 500 | 300 |
| T3 | S- Type (Microchannel) | 46 | 26.5 | 1.2 | 500 | 180 |
| T4 | I- Type (Microchannel) | 54 | 26.5 | 2 | 500 | 300 |

Table 2. Geometric parameters of the microchannel heat exchangers [3, 25].



a) S-type



b) I-type

Fig. 3. Dimensions of the test samples.

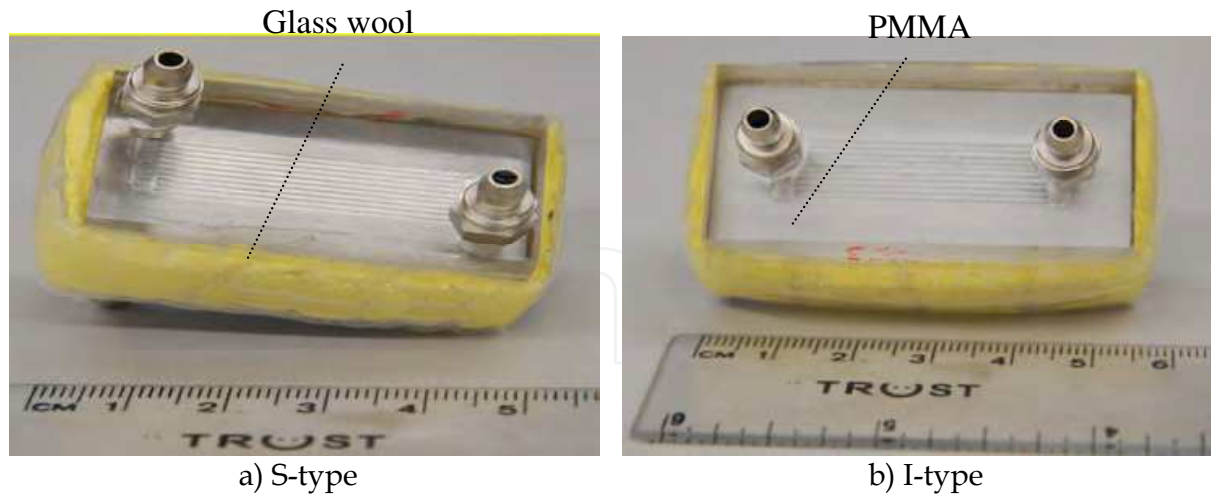


Fig. 4. Photos of the microchannel heat exchangers being tests.

| Material | Density kg/m ³ | Thermal conductivity W/(mK) |
|------------|---------------------------|-----------------------------|
| PMMA | 1420 | 0.19 |
| Glass wool | 154 | 0.051 |

Table 3. Physical properties of the PMMA and the glass wool [32].

Experimental data for the microchannel heat exchanger were obtained under the constant room temperature of 25 – 26 °C. DI water (deionized water) was used as the working fluid. Each inlet or outlet of the heat exchanger has a set of two thermocouples to record the temperature values, and there are eight thermocouples in total. At each side, a differential pressure transducer was used to measure the pressure drop. To assess the accuracy of measurements presented in this work, the uncertainty values for measured parameters are listed in Table 4. In addition, the uncertainties on the dimensions of microchannel evaluated by using a scanning laser made by Mitaka/Ryokosha model NH-3. The uncertainties of the scanning laser were estimated to be $\pm 0.03 \mu\text{m}$. Equipments used for the experiments are listed as follows [3, 22-31]:

1. Thermocouples, T-type
2. Pump, Model PU-2087, made by Jasco
3. Pump, VSP-1200, made by Tokyo Rikakikai
4. Heater, Model AXW-8, made by Medilab
5. Differential pressure transducer, Model PMP4110, made by Duck
6. Micro electronic balance, Model TE-214S, made by Sartorius.

| Parameter | Uncertainty |
|----------------|----------------------------------|
| Temperature | $\pm 0.1 \text{ }^\circ\text{C}$ |
| Pressure | $\pm 0.025\% \text{ FS}$ |
| Mass flow rate | $\pm 0.0015 \text{ g}$ |
| Channel height | $\pm 7 \mu\text{m}$ |
| Channel width | $\pm 10 \mu\text{m}$ |
| Channel length | $\pm 70 \mu\text{m}$ |

Table 4. Uncertainty data for measured parameters.

2.2 Analysis of data

In the following analyses, five assumptions were made:

- The fluid flow is laminar
- The fluid flow is incompressible and continuum
- Heat transfer is steady
- Radiation heat transfer is negligible
- Four heat exchangers were designed and fabricated by a precision micromachining process; as a result of this manufacturing process, roughness of microchannels was of the same order.

For the experiments carried out in this study, the effects of various parameters on the heat transfer and fluid flow – such as heat flux, effectiveness, pressure drop, and performance index – of the heat exchangers are discussed as follows.

The maximum heat transfer rate, Q_{max} , is evaluated by

$$Q_{max} = (mc)_{min} (T_{h,i} - T_{c,i}) \quad (1)$$

The heat transfer rate of the heat exchanger, Q , is calculated by

$$Q_c = m_c c_c (T_{c,o} - T_{c,i}) \quad (2)$$

The effectiveness (NTU method) is determined by

$$\varepsilon = \frac{Q_c}{Q_{max}} \quad (3)$$

Heat flux is calculated by

$$q = \frac{Q_c}{A} = \frac{m_c c_c (T_{c,o} - T_{c,i})}{n L_c W_c} \quad (4)$$

or

$$q = k \Delta T_{lm} = \frac{\Delta T_{lm}}{\Sigma R} \quad (5)$$

The overall thermal resistance ΣR is determined by

$$\Sigma R = R_{cond} + R_{conv} \quad (6)$$

The log mean temperature difference is calculated by

$$\Delta T_{lm} = \frac{\Delta T_{max} - \Delta T_{min}}{\ln \frac{\Delta T_{max}}{\Delta T_{min}}} \quad (7)$$

where m is mass flow rate (subscripts h and c stand for the hot side and cold side, respectively), n is number of microchannels, c is specific heat, $T_{h,i}$, $T_{h,o}$, $T_{c,i}$ and $T_{c,o}$ are inlet

and outlet temperatures of the hot and cold side, respectively, q is heat flux, A is heat transfer area, k is overall heat transfer coefficient, $R_{cond} = \delta / \lambda$ is conductive thermal resistance, $R_{conv} = 1 / h_h + 1 / h_c$ is convective thermal resistance, h_h and h_c are the convective heat transfer coefficients of the hot side and the cold side, respectively, δ is thickness of heat transfer, λ is thermal conductivity, and ΔT_{lm} is the log mean temperature difference.

The Reynolds number is calculated by:

$$\text{Re} = \frac{\rho w D_h}{\mu} = \frac{2m}{\mu(W_c + D_c)} \quad (8)$$

The pressure drop due to friction is determined by [33,34] :

$$\Delta p = 2f \rho w^2 \frac{L}{D_h} = 2f \text{Re} \frac{L}{D_h^2} w \mu \quad (9)$$

where $D_h = 4A_c / P$ is the hydraulic diameter, w is velocity in the z-direction, μ is dynamic viscosity, ρ is density, A_c is cross-sectional area, P is wetted perimeter, L is channel length, and f is Fanning friction factor.

The total pressure drop of the heat exchanger is given by

$$\Delta p_t = \Delta p_h + \Delta p_c \quad (10)$$

where Δp_h and Δp_c are pressure drops of hot and cold sides, respectively.

The performance index, ξ , is determined by [19, 25]

$$\xi = \frac{Q_c}{\Delta p_t} = \frac{m_c c_c (T_{c,o} - T_{c,i})}{\Delta p_h + \Delta p_c} \quad (11)$$

The experimental uncertainties were estimated, following the method described by Holman [35]; the final expressions for uncertainties were given as follows:

$$\frac{U_q}{q} = \left[\left(\frac{\partial m_c}{m_c} \right)^2 + \left(\frac{\partial c_c}{c_c} \right)^2 + \left(\frac{\partial T_{c,o} + \partial T_{c,i}}{T_{c,o} + T_{c,i}} \right)^2 + \left(\frac{\partial W_c}{W_c} \right)^2 + \left(\frac{\partial L_c}{L_c} \right)^2 \right]^{1/2} \quad (12)$$

$$\frac{U_k}{k} = \left[\left(\frac{\partial m_c}{m_c} \right)^2 + \left(\frac{\partial c_c}{c_c} \right)^2 + \left(\frac{\partial T_{c,o} + \partial T_{c,i}}{T_{c,o} + T_{c,i}} \right)^2 + \left(\frac{\partial W_c}{W_c} \right)^2 + \left(\frac{\partial L_c}{L_c} \right)^2 + \left(\frac{\partial T_{h,i}}{T_{h,i}} \right)^2 + \left(\frac{\partial T_{h,o}}{T_{h,o}} \right)^2 + \left(\frac{\partial T_{c,i}}{T_{c,i}} \right)^2 + \left(\frac{\partial T_{c,o}}{T_{c,o}} \right)^2 \right]^{1/2} \quad (13)$$

$$\frac{U_{\text{Re}}}{\text{Re}} = \left[\left(\frac{\partial m}{m} \right)^2 + \left(\frac{\partial \rho}{\rho} \right)^2 + \left(\frac{\partial \mu}{\mu} \right)^2 + \left(\frac{\partial W_c}{W_c} \right)^2 + \left(\frac{\partial D_c}{D_c} \right)^2 \right]^{1/2} \quad (14)$$

$$\frac{U_\varepsilon}{\varepsilon} = \left[\left(\frac{\partial m_c}{m_c} \right)^2 + \left(\frac{\partial c_c}{c_c} \right)^2 + \left(\frac{\partial m}{m} \right)^2 + \left(\frac{\partial c}{c} \right)^2 + \left(\frac{\partial T_{c,o} + \partial T_{c,i}}{T_{c,o} + T_{c,i}} \right)^2 + \left(\frac{\partial T_{h,i} + \partial T_{c,i}}{T_{h,i} + T_{c,i}} \right)^2 \right]^{1/2} \quad (15)$$

$$\frac{U_\xi}{\xi} = \left[\left(\frac{\partial m_c}{m_c} \right)^2 + \left(\frac{\partial c_c}{c_c} \right)^2 + \left(\frac{\partial T_{c,o} + \partial T_{c,i}}{T_{c,o} + T_{c,i}} \right)^2 + \left(\frac{\partial \Delta p_h}{\Delta p_h} \right)^2 + \left(\frac{\partial \Delta p_c}{\Delta p_c} \right)^2 \right]^{1/2} \quad (16)$$

By using the estimated errors of parameters listed in Table 3, the maximum experimental uncertainties in determining q , k , Re , ε , and ξ were 2.1%, 2.2%, 3.1%, 0.9%, and 3.3%, respectively, for all cases being studied.

3. Numerical simulation

Numerical study of the behavior of the microchannel heat exchanger with 3D single-phase fluid flow and heat transfer was done by using the COMSOL Multiphysics software, version 3.5. The algorithm of this software was based on the finite element method. For the COMSOL package, the generalized minimal residual (GMRES) method was used to solve for the model used in this study; the GMRES method was an iterative method for general linear systems. At every step, the method performed minimization of the residual vector in a Krylov subspace [32], and the Arnoldi iteration was used to find this residual vector. To improve the convergence of the iterative solver used by the GMRES method, the Incomplete LU (lower-upper) pre-conditioner was selected for nonsymmetric systems, where LU is a matrix which was the product of a lower triangular matrix and an upper triangular matrix. For the study, water was used as the working fluid. With the mass flow rate of water from 0.1667 to 0.8540 g/s, the Reynolds number was lower than 400 and the working fluid in the microchannels of the heat exchanger was under laminar flow condition [2]. No internal heat generation was specified, resulting in $Q_i = 0$. The finite elements in the grid meshes were partitioned to be triangular, as shown in Fig. 5. The maximum element size scaling factor was 1.9, with element growth rate of 1.7, mesh curvature factor of 0.8, and mesh curvature cut-off of 0.05. In Fig. 4, the schematic meshing of the heat exchanger consists of 26,151 mesh elements, the number of degrees of freedom is 76,411, and a relative tolerance is 10^{-6} .

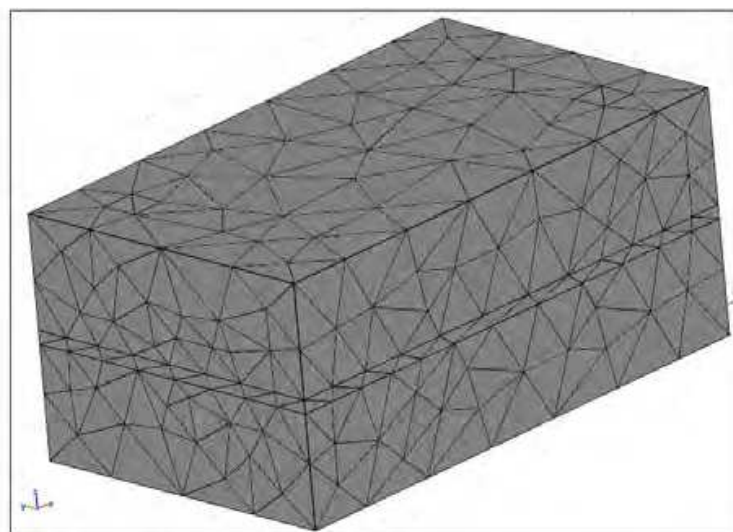


Fig. 5. Grid mesh diagram of the microchannel heat exchanger.

4. Results

4.1 Effects of fluid properties

For the effects of fluid properties on heat transfer and fluid flow behaviors, the microchannel heat exchanger T1 was tested; the results were shown more in detail by Dang et al. [26]. The parameters of heat exchangers are listed in Table 2.

Flow rate and inlet temperature being constant for the cold side

For experiments carried out in the study, the inlet temperature and mass flow rate of the cold side were fixed at 26.5 °C and 0.1773 g/s, respectively. For the hot side, an inlet temperature was fixed at 52 °C and the mass flow rates were varying from 0.1841 to 0.3239 g/s. The thermal boundary conditions of the top and bottom walls of the heat exchanger were assumed to be constant heat flux. The convective heat transfer coefficient between the wall and the ambient used for this solver was 10 W/(m²K), with the ambient temperature and air velocity of 26 °C and 0.2 m/s, respectively. The temperature profile of the microchannel heat exchanger is shown in Fig. 6 for a mass flow rate of 0.2556 g/s at the hot side.

At a constant inlet temperature of 52 °C at the hot side, for the case with both mass flow rate and temperature constant at the inlet of cold side, a relationship between the outlet temperatures (for both the hot side and cold side) and the mass flow rate of the hot side is shown in Fig. 7a. The outlet temperatures increase as the mass flow rate of the hot side increases. Because that the heat exchanger under study is the one with counter-flow, the outlet temperature of the cold side is higher than that obtained at the hot side [22-24]. A comparison between the numerical and experimental results is also shown in Fig. 7a. Fig 7a shows the outlet temperatures as a function of the mass flow rate of the hot side, and the results obtained from the simulation are in good agreement with those obtained from the experiments. The maximum difference of the outlet temperatures is 0.8 °C and the maximum percentage error is 2%.

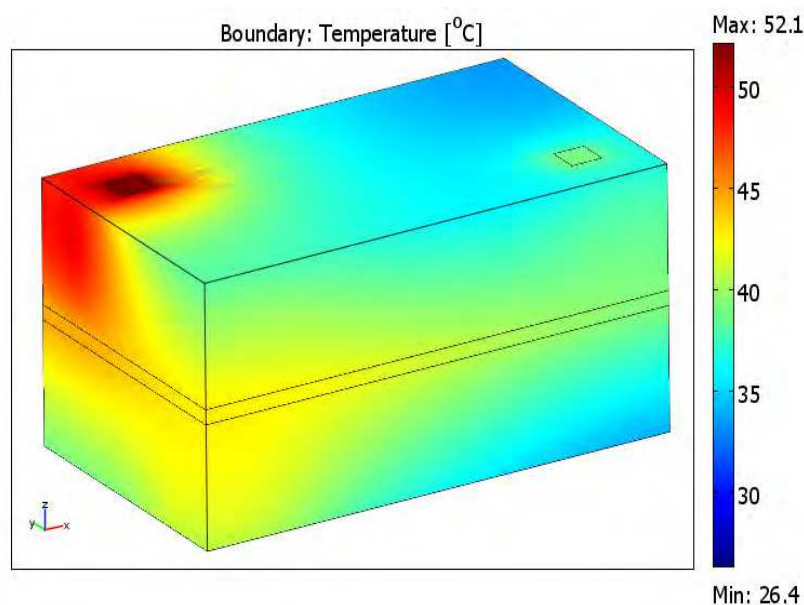


Fig. 6. The temperature profile of the microchannel heat exchanger.

At the condition stated above, the heat transfer rates of the hot side and cold side increase with rising mass flow rate of the hot side, as shown in Fig. 7b. The maximum difference of the heat transfer rate between the numerical results and experimental data is 1.08 W and the maximum percentage error is 7.3%. However, it is observed that the heat transfer rate for the hot side increases at a higher slope than that for the cold side as the mass flow rate increases. It is also observed that the actual effectiveness for the microchannel heat exchanger decreases with rising mass flow rate of the hot side, as shown in Fig. 7c. This means that the heat loss increases with rising flow rate of the hot side. Fig. 7c shows a relation of effectivenesses (actual effectiveness and NTU effectiveness) as a function of the mass flow rate of the hot side.

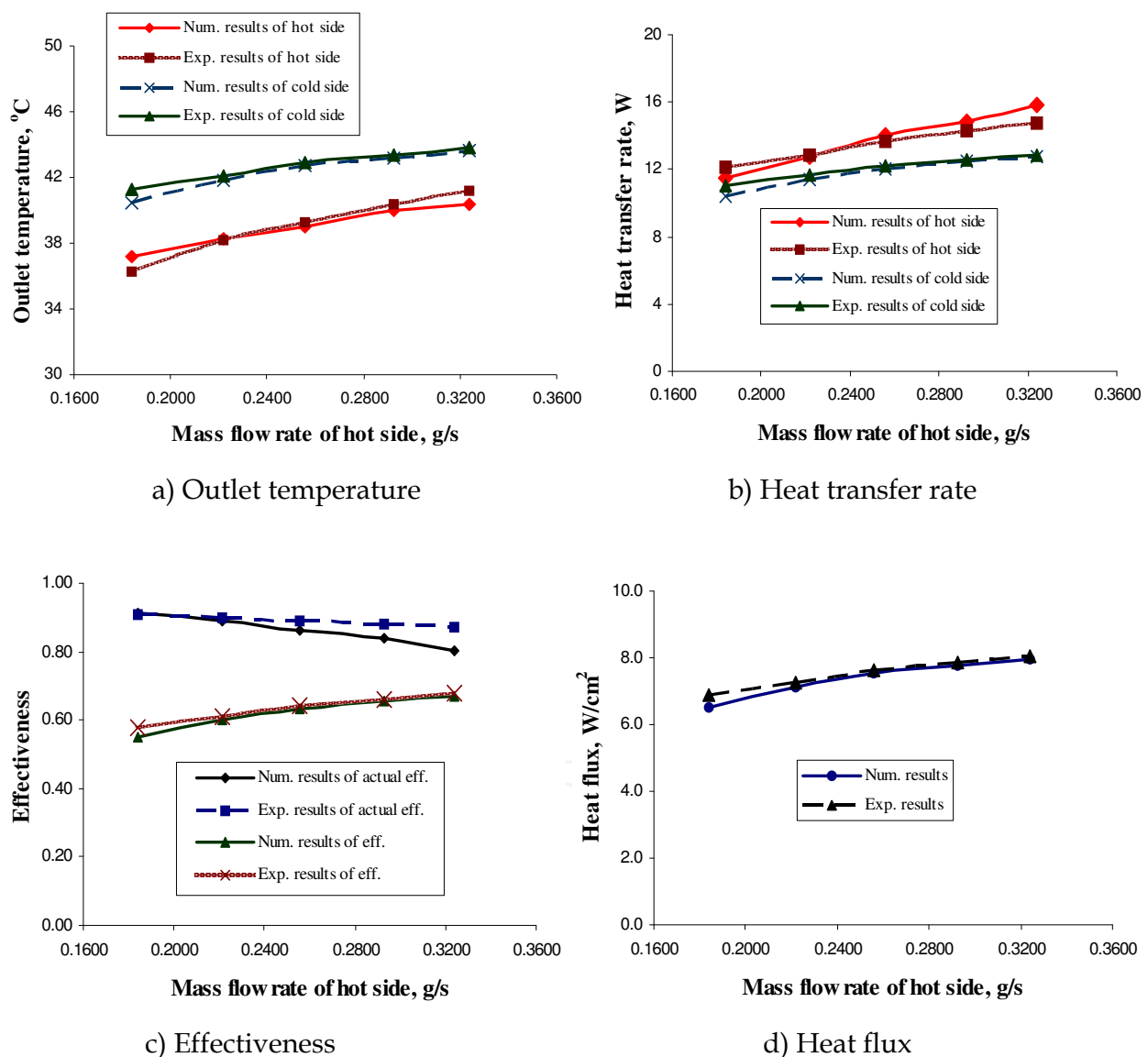


Fig. 7. A comparison between numerical and experimental results at constant inlet temperature and mass flow rate for the cold side.

Because that the inlet temperatures of both sides are fixed at constant values and that the heat capacity rate $(mc)_{min}$ is fixed, the maximum heat transfer Q_{max} is fixed at a constant

value, as shown in Eq. (6). When the mass flow rate of the hot side is increased, the heat transfer rate Q of the heat exchanger increases also. As a result, heat transfer obtained from the effectiveness increases with a rising the mass flow rate at the hot side. The trends of effectiveness and actual effectiveness are observed to be in the opposite directions, as shown in Fig. 7c.

The results obtained from numerical simulation and from experimental data for the actual effectiveness and for the effectiveness are compared also. Fig. 7c indicates that at various mass flow rates of the hot side, the heat transfer results obtained from the actual effectivenesses are higher than those obtained from the effectivenesses. The maximum difference of the effectivenesses between the two occurs at high mass flow rate of the hot side, with the maximum difference of 0.7 and the maximum percentage error of 8.7 %. This difference may be due to errors in the experiments or mesh generation in the numerical simulations. It is noted that experimental results of effectiveness obtained from this study are higher than those obtained from Kang and Tseng [6].

Again, at the condition stated above, the heat flux of the microchannel heat exchanger increases from 5.8 to 8.0 W/cm² with a rising the mass flow rate of the hot side ranging from 0.1841 to 0.3239 g/s, as shown in Fig. 7d. A comparison between the numerical and experimental results for the heat flux at various mass flow rates of the hot side is shown in Fig. 7d. Since the heat flux obtained from the simulation is only slightly higher than that obtained from the experiment, the results obtained from the simulation are judged to be in good agreement with those obtained from the experiments. The maximum difference of heat fluxes is 0.40 W/cm²; it occurs at low mass flow rate of the hot side, and the maximum percentage error is 7.2%. This difference may be due to errors in the experiments or mesh generation in the numerical simulations also. The heat flux obtained from this study is higher than that obtained from [5]; the latter has the heat flux increasing from 0.2 to 1.1 W/cm² and the mass flow rate increasing from 2.7 to 111.1 g/s. However, due to the variation in presenting data, it is difficult to make a complete comparison between the results obtained from the present study and those obtained from [5] and [7].

To summarize, for this case with the results presented in Figs. 7a-7d, the trends for actual effectiveness and effectiveness indicate that as the mass flow rate of hot side goes up, the former goes down while the latter goes up; this is an important effect observed for the microchannel heat exchanger used in the study.

Flow rate and inlet temperature being constant for the hot side

For this case, the inlet temperature and mass flow rate of the hot side were fixed at 52 °C and 0.1667 g/s, respectively. For the cold side, an inlet temperature was fixed at 26.5 °C and the mass flow rates were varying from 0.1859 to 0.3625 g/s. Fig. 8a shows a relationship between the outlet temperatures (for both the hot side and cold side) and the mass flow rates of the cold side at the condition stated above. Contrary to the category of cases of constant mass flow rate and inlet temperature for the cold side, the outlet temperatures decrease as the mass flow rate of the cold side increases. A comparison between the results obtained from numerical simulation and experimental data for the outlet temperatures of both the hot side and the cold side is shown in Fig. 8a. The maximum difference between the two results is 0.4 °C, occurring at low mass flow rate of cold side, with the maximum percentage error of 1.2%.

It is observed that with a rising the mass flow rate of the cold side, the outlet temperatures decrease, as shown in Fig. 8a; however, for the same flow rate condition, both the heat transfer rates of the hot side and cold side increase. As the mass flow rate of the cold side increases, the heat transfer rate for the cold side increases at a slightly higher rate than that for the hot side. It is also observed that the actual effectiveness for the microchannel heat exchanger increases with a rising the mass flow rate of the cold side, as shown in Fig. 8b. The results obtained from the effectiveness (NTU method) are lower than those obtained from the actual effectiveness, as shown in Fig. 8.b. Hence, a conclusion can be drawn for the heat exchanger under study: at constant inlet temperature and mass flow rate of the hot side, it is more effective to use the heat exchanger with high mass flow rate of cold side. However, leakage of liquid out of the microchannel heat exchanger can occur when the mass flow rate of the cold side increases above 0.854 g/s, as a result of the excessive pressure exerted on the system under study.

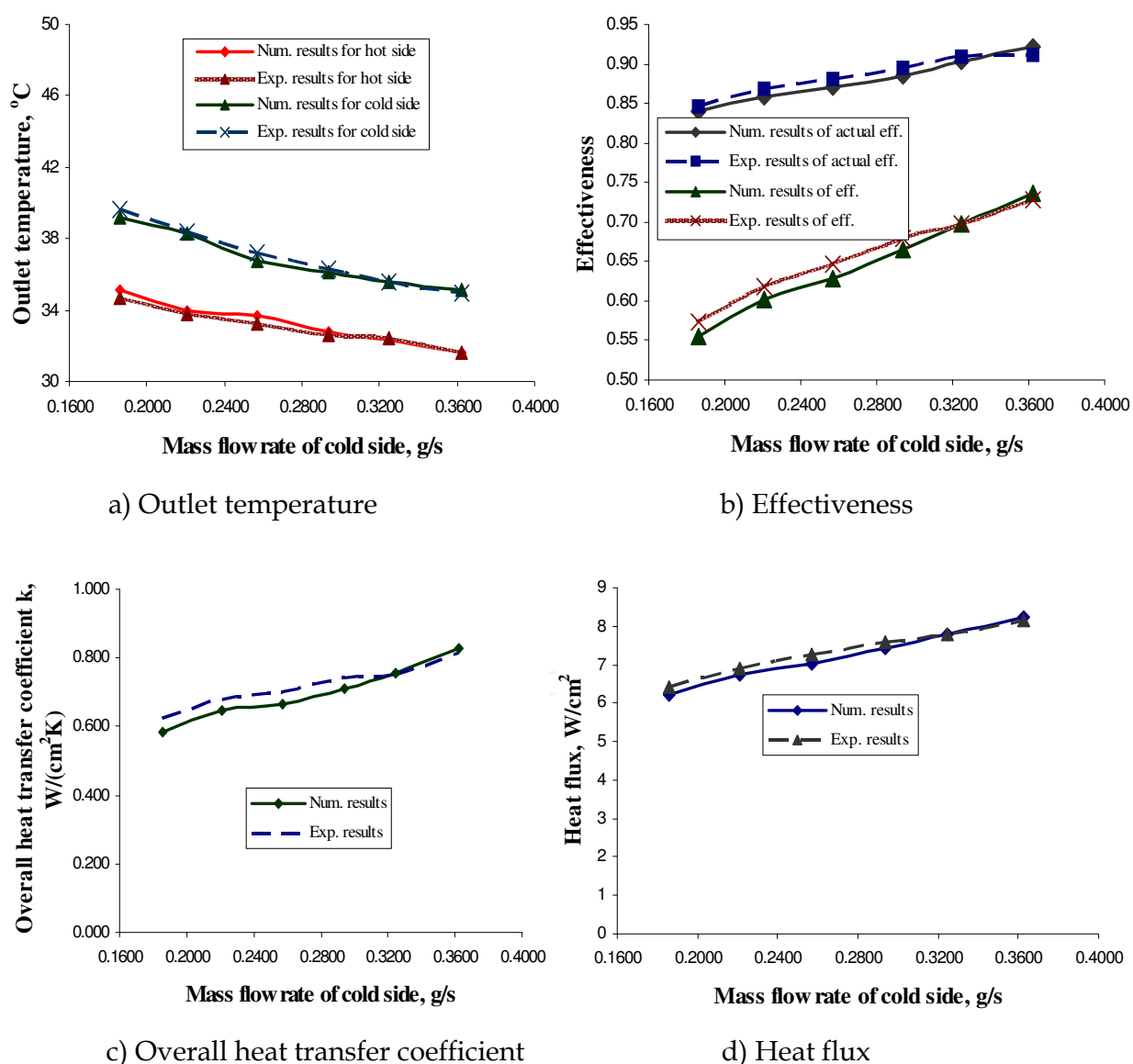


Fig. 8. Comparison between numerical and experimental results at constant inlet temperature and mass flow rate for the hot side.

At the condition stated above, the overall heat transfer coefficient k of the heat exchanger increases from 0.625 to 0.815 W/(cm²K) with the mass flow rate of cold side rising from 0.1859 to 0.3625 g/s, as shown in Fig. 8c. At a hydraulic diameter of 375 μ m, Kandlikar et al. [44] gave $k = 0.85$ W/(cm²K), compared to $k = 0.815$ W/(cm²K) obtained in this study. Thus, the two results are in good agreement. For this case, the change in the log mean temperature difference is small: it reduces from 10.7 to 10.0 $^{\circ}$ C with the mass flow rate of cold side rising from 0.1859 to 0.3625 g/s. The heat flux increases from 6.2 to 8.2 W/cm² with the mass flow rate of cold side rising from 0.1859 to 0.3625 g/s, as shown in Fig. 8d. Thus, the heat flux affected by the log mean temperature difference is less than that by the overall heat transfer coefficient (7.0% versus 30.4% on a percentage basis). Comparisons between the results obtained from numerical simulation and experimental data for the outlet temperature, the effectiveness, the overall heat transfer coefficient, and the heat flux at various mass flow rates of the cold side are shown in Figs. 8a-8d, respectively, with the maximum percentage error being less than 7.2%.

Fluid behaviors

The boundary conditions of the two outlets of the hot side and the cold side are at the atmospheric pressure. Fig. 9 shows the velocity field along channels of the microchannel heat exchanger. The streamlines of water pass from the microchannels to the manifold. At the edge between channels and manifold, the streamlines appear to be curved in shape. The velocity field at the outlet of the manifold is parabolic which is consistent with that predicted by the laminar flow theory for fluid in a channel.

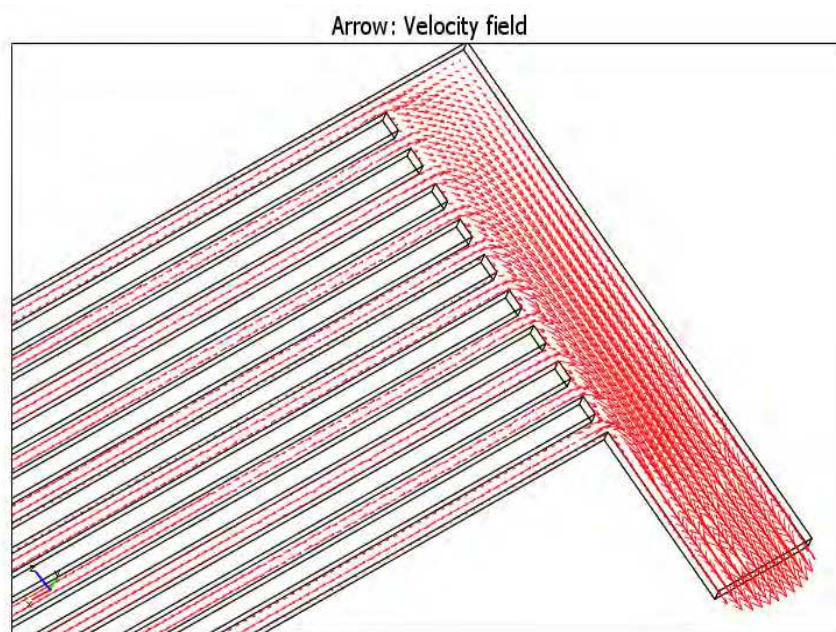


Fig. 9. The velocity field along channels of the microchannel heat exchanger.

Fig. 10 shows the pressure distribution in channels of the hot side at the mass flow rate of 0.2321 g/s and the inlet temperature of 45 $^{\circ}$ C. The pressure decreases gradually from the first channel to the last one, with the first channel being the nearest one to the entrance of the inlet of the manifold [25, 26].

For microchannel heat exchanger used in this study, at an inlet temperature of 25 °C, the pressure drop increases from 889 to 4,411 Pa, with the mass flow rate rising from 0.1812 to 0.8540 g/s. In addition, the pressure drop decreases as the inlet temperature increases, since as the inlet temperature increases, the dynamic viscosity decreases. Because that the Poiseuille number ($Po = f Re$) depends only on the geometry of the microchannel, the pressure drop decreases with a rising inlet temperature of water. This conclusion is in agreement with [6]. Fig. 11 shows the pressure drop obtained experimentally as a function of the inlet water temperature for various mass flow rates. At a mass flow rate of 0.4972 g/s, the pressure drop decreases from 2,437 to 1,776 Pa, with the inlet temperature rising from 25 °C to 52 °C.

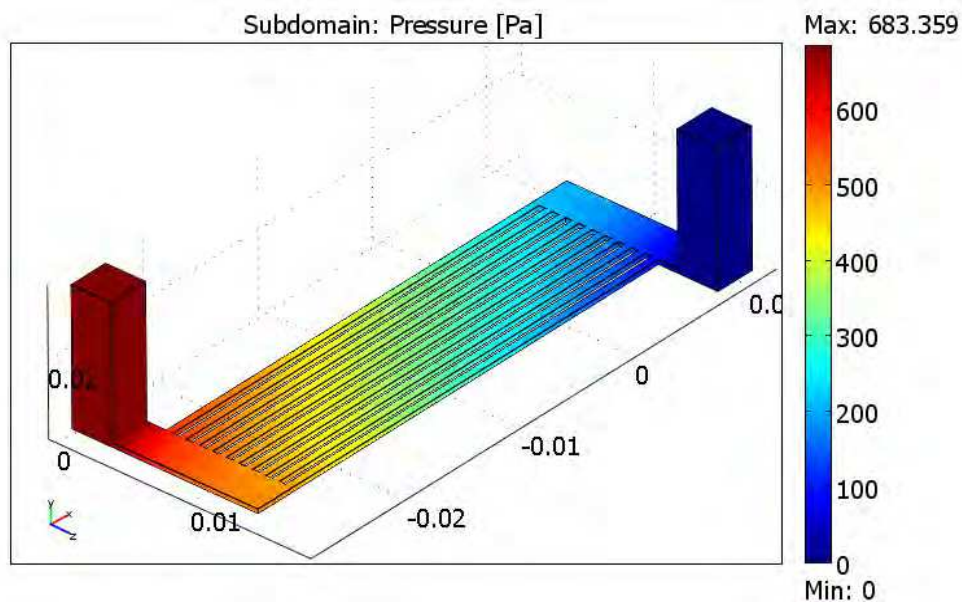


Fig. 10. Pressure distribution of the hot side of the heat exchanger.

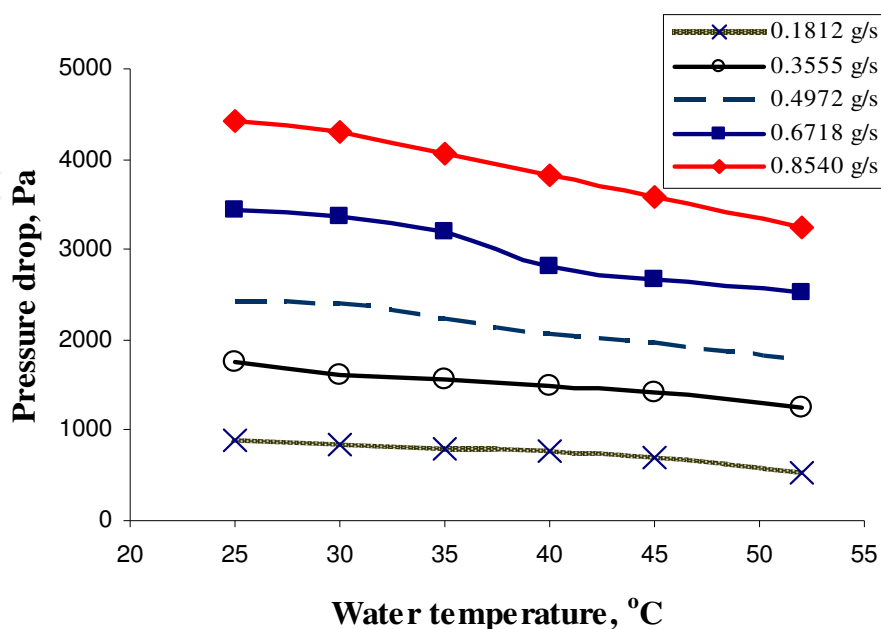


Fig. 11. Pressure drop as a function of the inlet water temperature for various mass flow rates.

Fig. 12 shows a comparison between numerical and experimental results for the pressure drops and the mass flow rates at various inlet water temperatures. As shown in the figure, the pressure drop decreases as the inlet water temperature increases. The maximum difference between the two results obtained is 131 Pa, with a maximum percentage error of 7.8%.

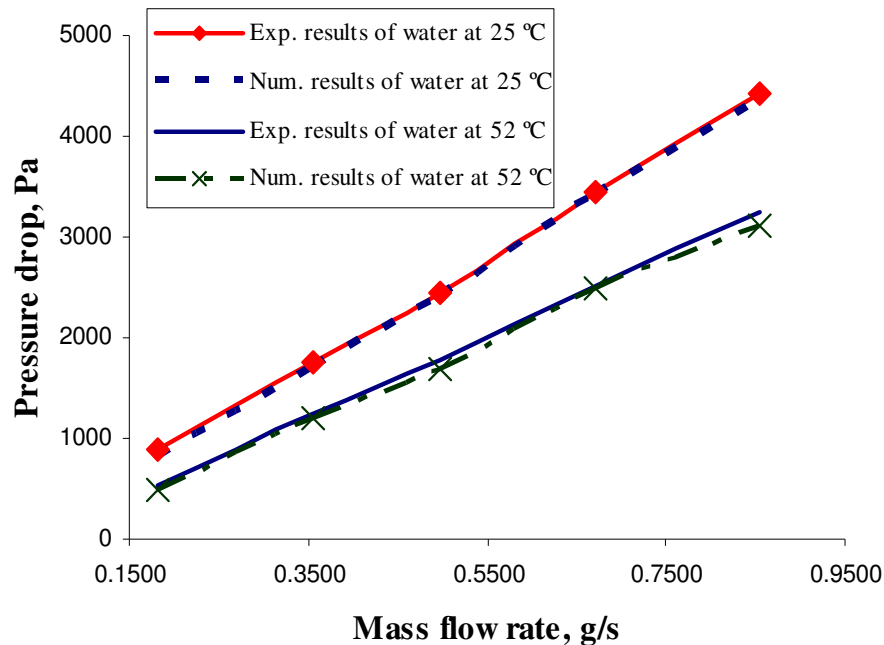


Fig. 12. Comparison between numerical and experimental results for the pressure drop and the flow rate at various inlet water temperatures.

Under various conditions for all cases studied up to now, the maximum percentage errors between the results obtained from numerical simulations and those from experimental data are found to be less than 9% and are in good agreement.

4.2 Effects of flow arrangements

For this section, single-phase heat transfer and fluid flow phenomena obtained from experimental data and numerical simulations for the microchannel heat exchanger T1 were investigated. Two cases of flow arrangements will be discussed for the heat exchanger under investigation: (1) the counter-flow arrangement and (2) the parallel-flow arrangement. The dimensions of this microchannel heat exchanger are shown in Fig 3 and its geometric parameters are listed in Table 2. The conditions of the numerical simulation and experimental data are indicated in more detail in [3, 22-25].

For the experiments carried out in this section, the inlet temperature and the mass flow rate of the cold side were fixed at 22.5 °C and 0.2043 g/s, respectively. For the hot side, the mass flow rate was fixed at 0.2321 g/s and the inlet temperatures were varying from 45 to 70 °C (Dang et al. [26]). The thermal boundary conditions of the top and bottom walls of the heat exchanger are assumed to be constant heat flux. The temperature profile of the microchannel heat exchanger is shown in Fig. 13 for the inlet temperature of 45 °C at the hot

side. Fig. 13a and Fig. 13b show the temperature profiles for the cases with counter-flow and parallel-flow at the conditions specified above.

The 3D temperature profiles of the microchannel heat exchanger were shown in more detail in [24-26] also. Profiles of the temperature gradients shown in Fig. 14 indicate the temperature gradients from heat exchanger's cold region towards its hot region, with Fig. 14a being the counter-flow and Fig. 14b being the parallel-flow. Distribution of the temperature gradients varies along the channel length of the heat exchanger with counter-flow and parallel-flow configurations. In the middle of the heat exchanger with counter-flow arrangement, the temperature gradients are in fishbone shapes. However, the temperature gradients are in the perpendicular direction towards the substrate of the heat exchanger with parallel-flow arrangement.

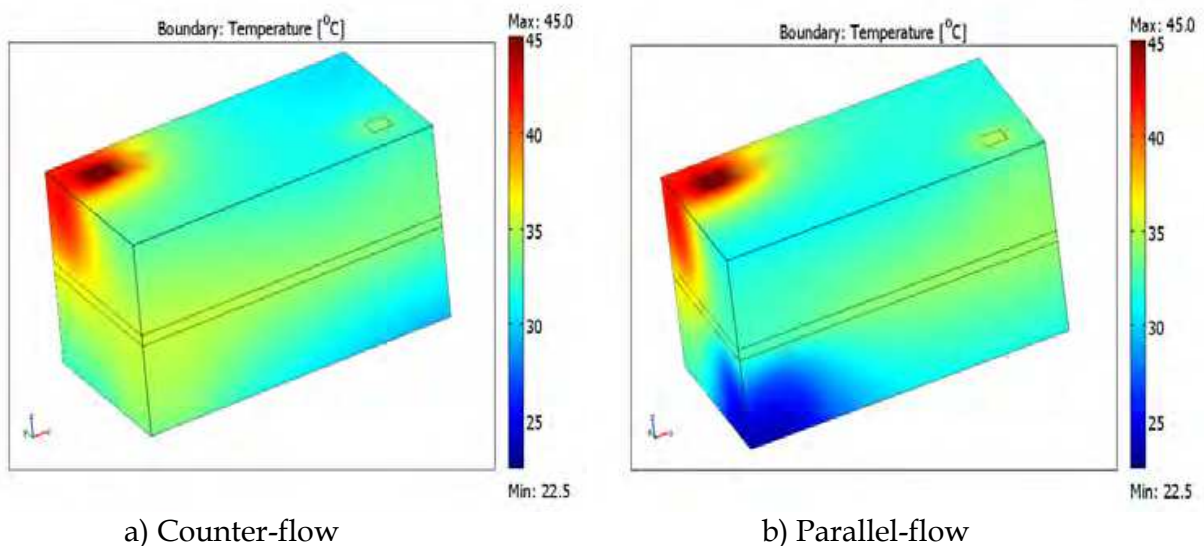


Fig. 13. Temperature profiles of the microchannel heat exchanger.

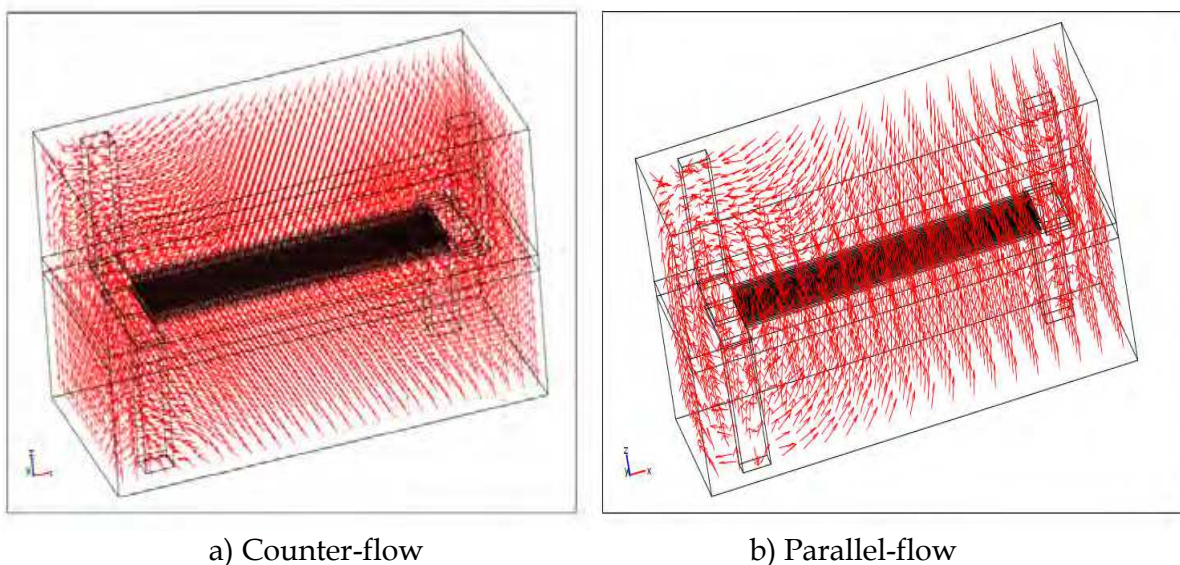


Fig. 14. The profiles of temperature gradients of the microchannel heat exchanger.

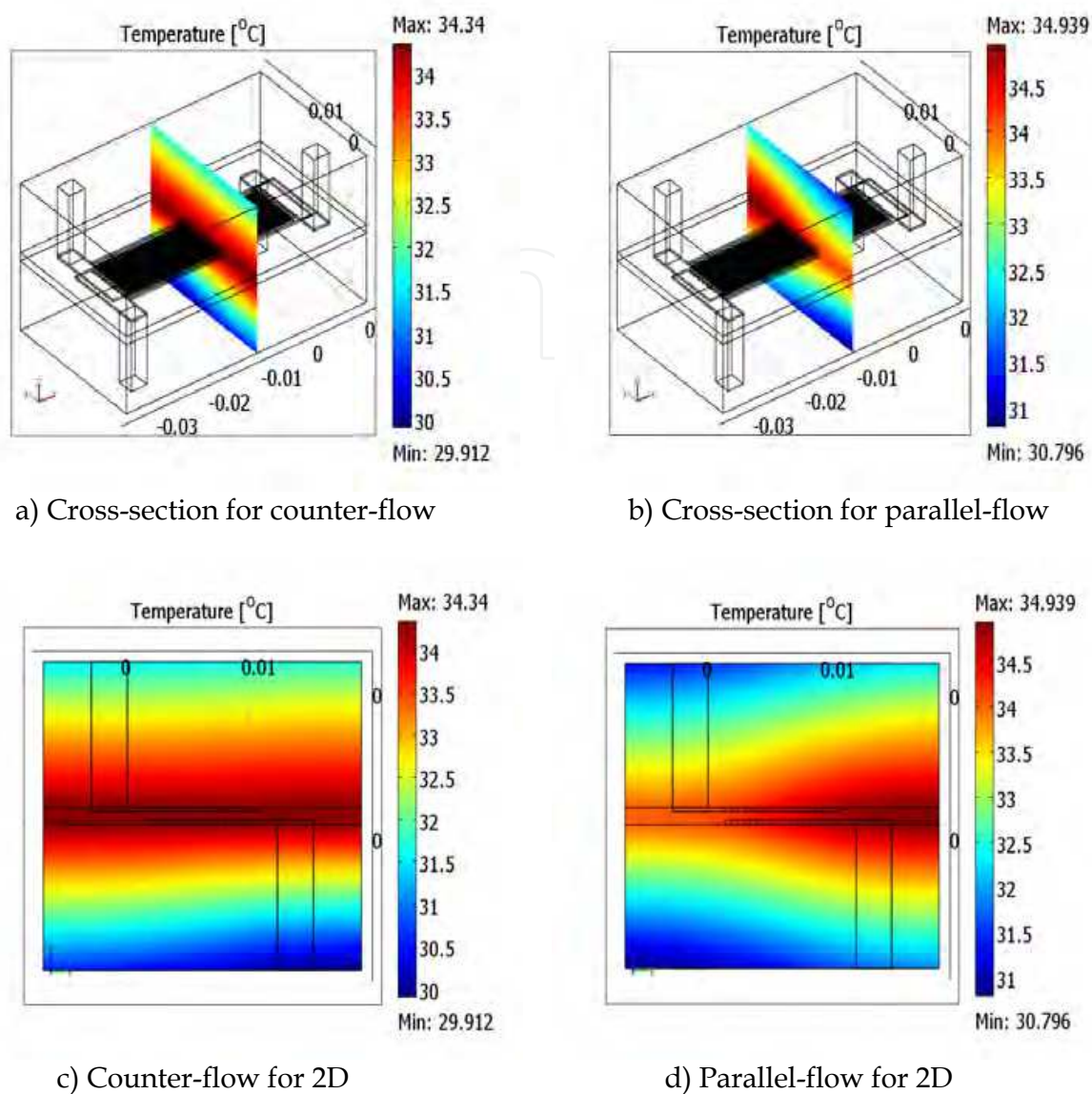


Fig. 15. Temperature profiles of a cross-section of the microchannel heat exchanger.

The temperature profiles of the microchannel heat exchanger are shown in Fig. 15 for the inlet temperature of 45 °C at the hot side at the cross-section through three points: $(-0.01, 0.02, -0.02)$, $(-0.01, 0.02, 0.00)$, and $(-0.01, 0, 0.00)$. Fig. 15a and Fig. 15b show the temperature profiles of the cross-section in the microchannel heat exchanger for the cases with counter-flow and parallel-flow at the conditions specified above. At this cross-section, it is observed that the temperature profiles varying along the distance measured from the substrate for counter-flow arrangement are more evenly distributed (as shown in Fig. 15c) than those for parallel-flow arrangement with the hot temperature region skewed to the right-side of the microchannel, as shown in Fig. 15d.

As a result, the range of temperature gradient obtained from counter-flow arrangement is smaller than that obtained from parallel-flow one. For the counter-flow one, the temperature gradients obtained numerically ranging from 50.3 to 529.1 K/m, as shown in Fig. 16a. However, the range is from 16.6 to 574 K/m for parallel-flow one, as shown in Fig. 16b. The

profiles of the temperature gradients in 3D and in these three planes (x-y, y-z, and z-x planes) for the whole subdomains of the heat exchanger were shown in more detail in [24-26].

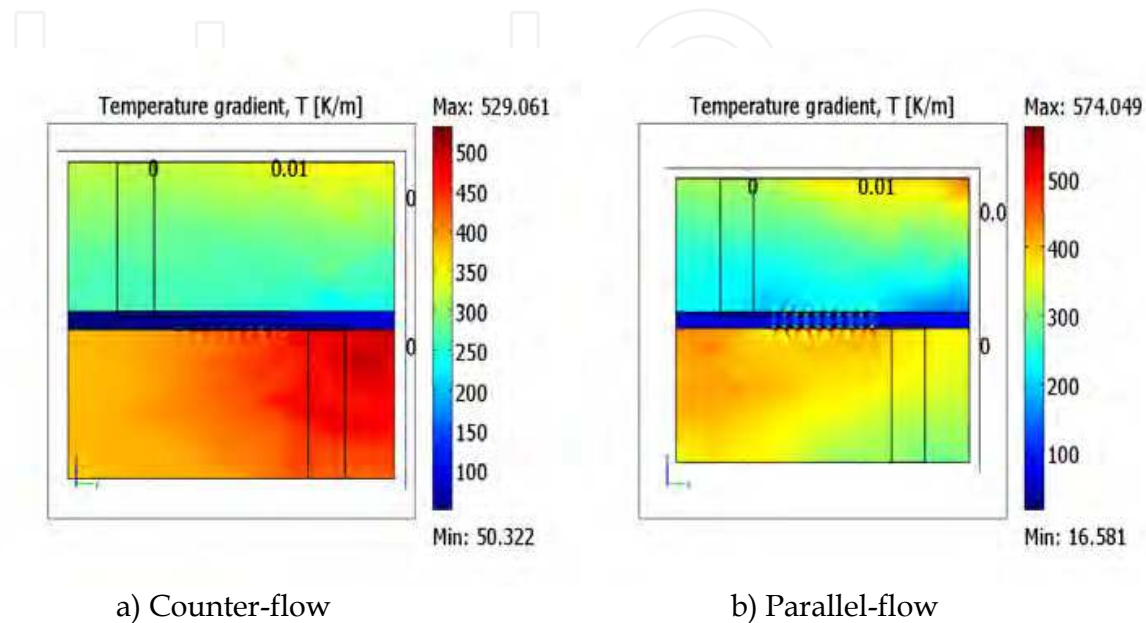


Fig. 16. Profiles of 2D temperature gradients of the microchannel heat exchanger.

Under the condition stated above, the inlet temperature and the mass flow rate of the cold side were fixed at 22.5 °C and 0.2043 g/s, respectively. For the hot side, the mass flow rate was fixed at 0.2321 g/s and the inlet temperatures were varying from 45 to 70 °C [22-25]. A relationship of the experimental results between the counter-flow and the parallel-flow cases is shown in Fig. 17.

For the counter-flow case, the outlet temperature at the cold side is higher than that obtained at the hot side (see Fig. 17a). However, for the parallel-flow case, the outlet temperature at the cold side is lower than that obtained at the hot side. As a result, the heat transfer rate obtained from the counter-flow arrangement is higher than that obtained from the parallel-flow arrangement of the microchannel heat exchanger, as shown in Fig. 17b. It is noted that to compute the heat transfer rates for an adiabatic heat exchanger, these rates were based on those of the cold side. Fig. 17c shows the comparison of pressure drops of both cases for the counter- and parallel-flow arrangements. It is observed that the pressure drop obtained from the hot side is higher than that obtained from the cold side; this is consistent with the fact that the mass flow rate of the hot side is also higher than that of the cold side. It is also observed that the pressure drop obtained from the counter-flow arrangement is the same as that obtained from parallel-flow one. As a result, the performance index obtained from the counter-flow arrangement is higher than that obtained from the parallel-flow one: the value obtained from the counter-flow is 1.192 to 1.2 times of that obtained from the parallel-flow, as shown in Fig. 17d.

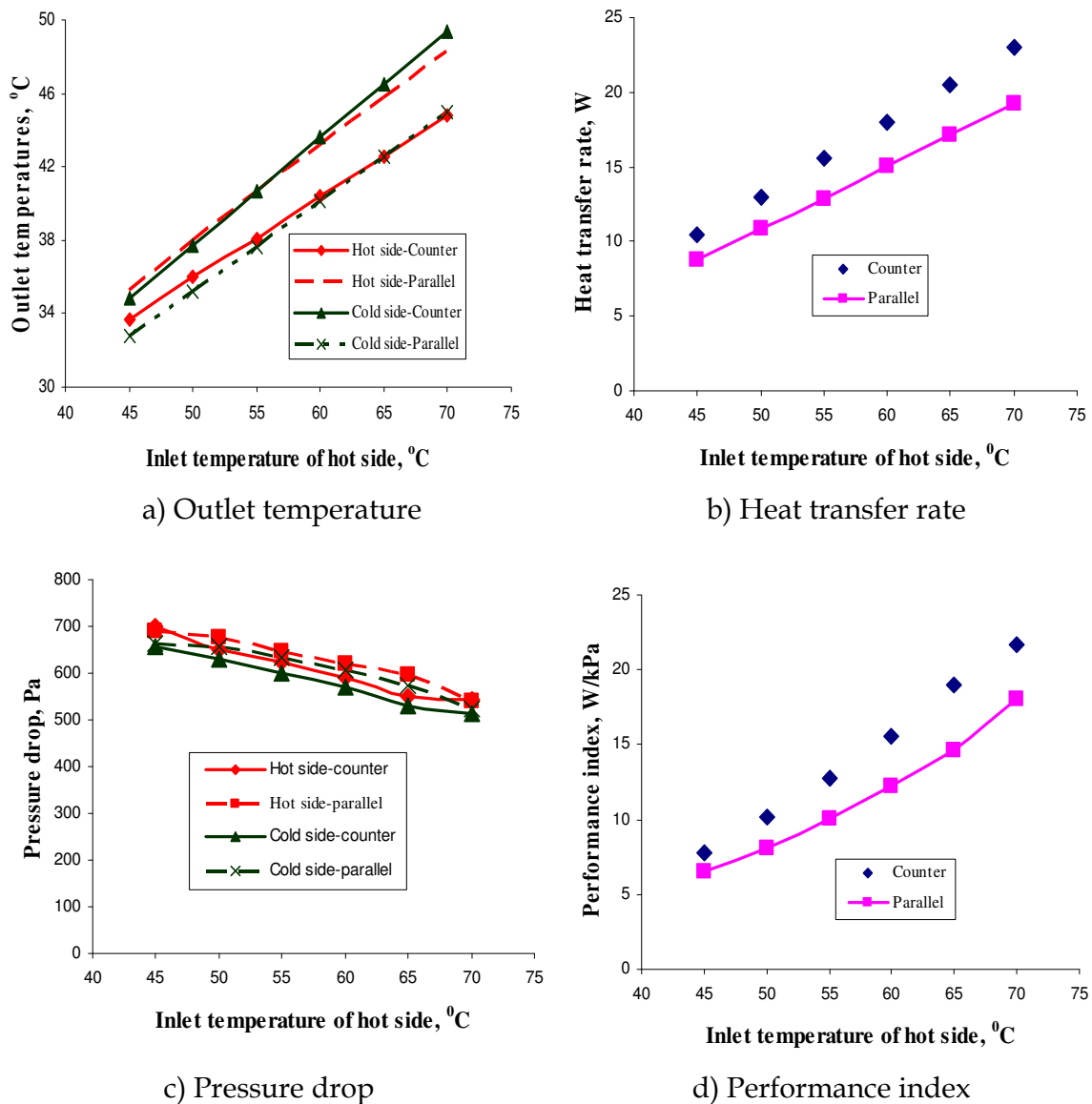


Fig. 17. Comparison of the experimental results between the counter-flow and parallel-flow.

When the inlet temperature of the hot side is increased, the heat transfer rate Q of the heat exchanger increases also. As a result, the heat transfer result obtained from the effectiveness (NTU method) increases with rising inlet temperature at the hot side, as shown in Fig. 18a. The figure shows a comparison between numerical and experimental results of the effectiveness (NTU method) for the microchannel heat exchanger with counter-flow arrangement. The maximum difference of the effectiveness is 0.009; it occurs at low inlet temperature of the hot side, and the maximum percentage error is 1.6%. Fig. 18b shows the comparison of the performance indexes between the numerical and experimental results for the case with counter-flow arrangement. Since the performance index obtained from the simulation is in the vicinity of that obtained from the experiment, the results obtained from the simulation are judged to be in good agreement with those obtained from the experiments. The maximum difference of the performance index is 0.413 W/kPa; it occurs at low inlet temperature of the hot side for the counter-flow arrangement, and the maximum percentage error is 5.3%.

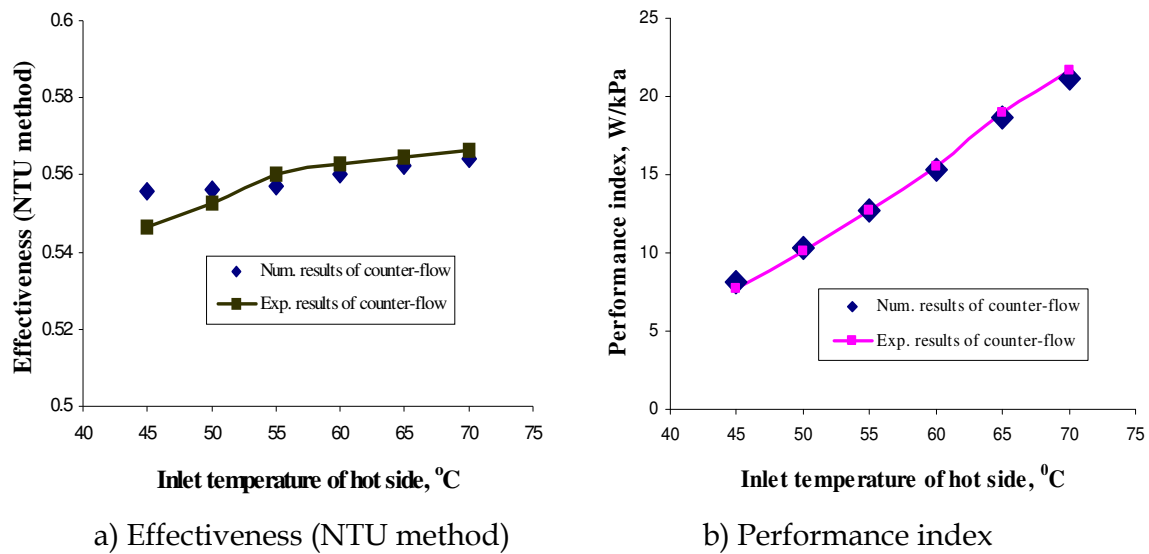


Fig. 18. Comparison between numerical and experimental results.

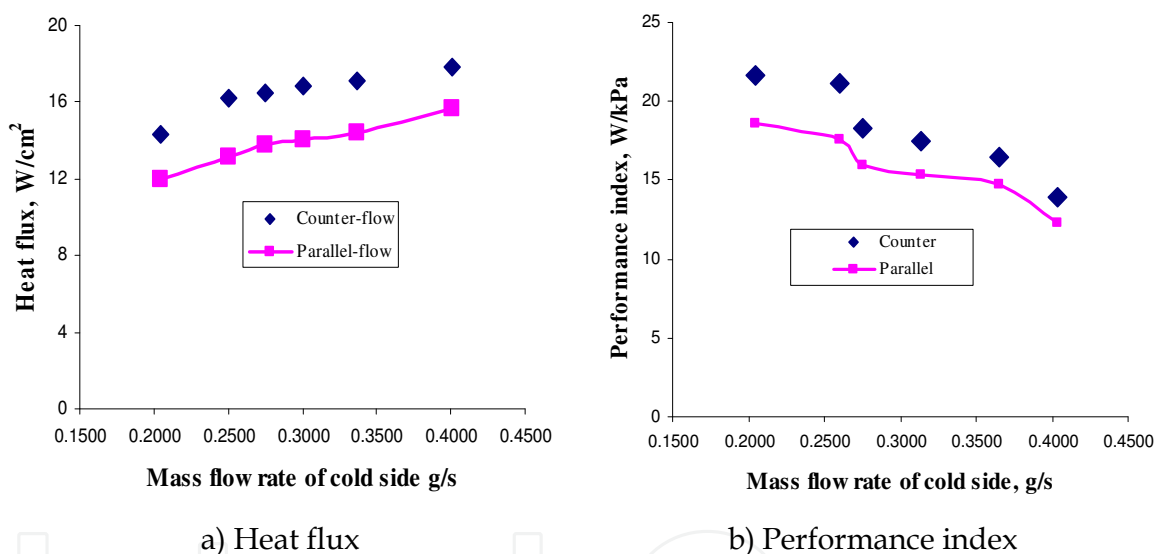


Fig. 19. Comparison of the experimental results with a rising mass flow rate of the cold side.

Under another experimental condition, for the experiments done in this study, the inlet temperature and the mass flow rate of the hot side were fixed at 70 °C and 0.2321 g/s, respectively. For the cold side, the inlet temperature was fixed at 22.5 °C and the mass flow rates were varying from 0.2043 to 0.401 g/s. The outlet temperatures are a function of the mass flow rate at the cold side, as shown in more detail in [22-25]. Contrary to the case of varying inlet temperature of the hot side, the outlet temperatures decrease as the mass flow rate of the cold side increases. For the counter-flow case, the outlet temperature of the cold side is higher than or equal to that obtained at the hot side. However, for the parallel-flow case, the outlet temperature at the cold side is lower than that obtained at the hot side. As a result, for the microchannel heat exchanger, the heat flux obtained from the counter-flow arrangement is higher than that obtained from the parallel-flow arrangement, as shown in Fig. 19a. The heat flux of 17.81×10^4 W/m² (or 17.81 W/cm²) was achieved for water from the

hot side of the device having the inlet temperature of 70 °C and mass flow rate of 0.2321 g/s and for water from the cold side having the inlet temperature of 22.5 °C and mass flow rate of 0.401 g/s.

Fig. 19b shows the comparison of the performance indexes between the counter- and parallel-flow arrangements. The performance index obtained from the counter-flow arrangement is higher than that obtained from the parallel-flow one: the value obtained from the counter-flow is 1.13 to 1.17 times of that obtained from the parallel-flow. The performance index of 21.69 W/kPa was achieved for water from the hot side of the device having the inlet temperature of 70 °C and the mass flow rate of 0.2321 g/s and for water from the cold side having the inlet temperature of 22.5 °C and the mass flow rate of 0.401 g/s.

4.3 Effects of geometrical configurations

In order to study the effects of geometrical configurations on the performance of the heat exchangers, all experimental conditions for the four microchannel heat exchangers were kept the same, more detail in [28,29]. Throughout the section, two cases of testing were discussed: the first one for increasing the inlet temperature of the hot side and the second for increasing the mass flow rate of the cold side. Further details of these cases are as follows:

1. Case No. 1 is for the case of increasing the inlet temperature of the hot side: the inlet temperature and the mass flow rate of the cold side were fixed at 22.5 °C and 0.2135 g/s, respectively; at the hot side, the mass flow rates was fixed at 0.2308 g/s and the inlet temperature were varying from 45 to 70 °C.
2. Case No. 2 is for the case of increasing the mass flow rate of the cold side: the inlet temperature and the mass flow rate of the hot side were fixed at 70 °C and 0.2308 g/s, respectively; at the cold side, the inlet temperature was fixed at 22.5 °C and the mass flow rates were varying from 0.2135 to 0.401 g/s.

The flow parameters for these two cases are summarized in Table 5.

| Case | Flow conditions | |
|------|--|--|
| | Variable parameters | Fixed parameters |
| 1 | $T_{h,i} = 45 \div 70 \text{ } ^\circ\text{C}$ | $m_h = 0.2308 \text{ g/s}$ $m_c = 0.2135 \text{ g/s}$ $T_{c,i} = 22.5 \text{ } ^\circ\text{C}$ |
| 2 | $m_c = 0.2135 \div 0.401 \text{ g/s}$ | $m_h = 0.2308 \text{ g/s}$ $T_{h,i} = 70 \text{ } ^\circ\text{C}$ $T_{c,i} = 22.5 \text{ } ^\circ\text{C}$ |

Table 5. Flow parameters for the cases under study.

The effects of substrate thicknesses

For the effects of substrate thicknesses, the two microchannel heat exchangers (T1 and T2) were tested. These two heat exchangers have the same dimensions of the channel and the manifolds with the same means (that is, the S-type, as shown in Fig. 3a)) for connecting the channels to the manifolds; however, the two heat exchangers under study have different substrate thicknesses. Detailed parameters of the heat exchangers (T1 and T2) are listed in Table 2.

Fig. 20 shows the effects of the substrate thickness with rising inlet temperature of the hot side. The heat flux is a function of the inlet temperature of hot side; the heat flux increases with rising inlet temperature of the hot side, as shown in Fig. 20a. For the substrate thicknesses of 1.2 (Heat Exchanger T1) and 2 mm (Heat Exchanger T2), the heat fluxes of T1 are 1.024 to 1.046 times of those obtained from T2. Besides, it was found that the heat transfer rate obtained from the present study (23 W) is slightly higher than that obtained from García-Hernando et al. [36] (22 W) (At Reynolds number of 400, the present study used the overall channel size with 9.5 mm in width and 32 mm in length (304 mm² in area), compared with that of 20 mm in width and 16 mm in length (320 mm² in area) for García-Hernando et al. [36]). It was also found for the present study that the heat transfer rate increases with rising inlet temperature of the hot side. As a result, the effectiveness – defined as the ratio of heat transfer rate to the maximum heat transfer rate, expressed by Eq. (3) – increases with rising inlet temperature of the hot side, as shown in Fig. 20b. Because that the configuration of the heat exchangers and the mass flow rates of water at the hot and cold sides are fixed and the variation of temperature of water at both side is minimal, so the convective heat transfer term is essentially fixed. Further, it is found that the conductive heat transfer term does not affect strongly the overall heat transfer coefficient of the heat exchangers. It is concluded that the results shown in Figs. 20a and 20b indicate that the substrate thickness affects negligibly the parameters associated with the heat transfer process of the heat exchangers with the substrate thicknesses of 1.2 and 2 mm.

For the present study, the results obtained from the experimental data showed the pressure drop as a function of the inlet temperature of the hot side. For both heat exchangers (T1 and T2), the mass flow rate of the hot side is higher than those of the cold side, so the pressure drop obtained from the hot side is higher than that obtained from the cold side, as shown in Fig. 20c. Fig. 20c illustrates that pressure drop of T2 is not the same as that of T1, due to the fact that the roughness of channels in T2 could be higher than that of channels in T1. However, the maximum difference of pressure drops between T1 and T2 is less than 10 %.

Fig. 20d shows that the performance of the heat exchangers increase with the rising of inlet temperature of the hot side; the performance obtained from T1 is higher than that obtained from T2. The performance index of 21.67 W/kPa was achieved for water from the hot side of Heat Exchanger T1 having the inlet temperature of 70 °C and mass flow rate of 0.2308 g/s and water from the cold side having the inlet temperature of 22.5 °C and mass flow rate of 0.2135 g/s.

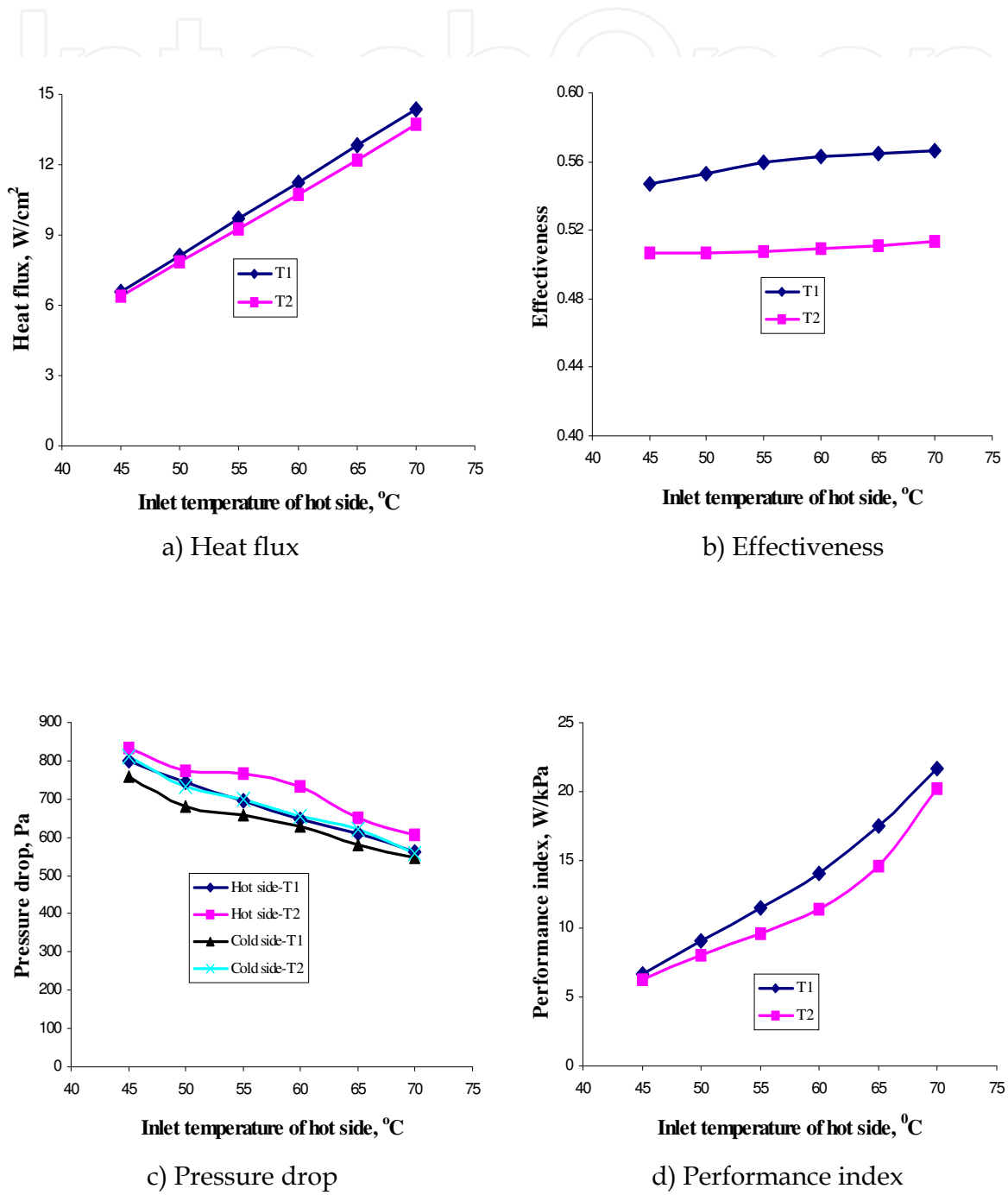


Fig. 20. Effects of the substrate thickness with a rising inlet temperature of hot side.

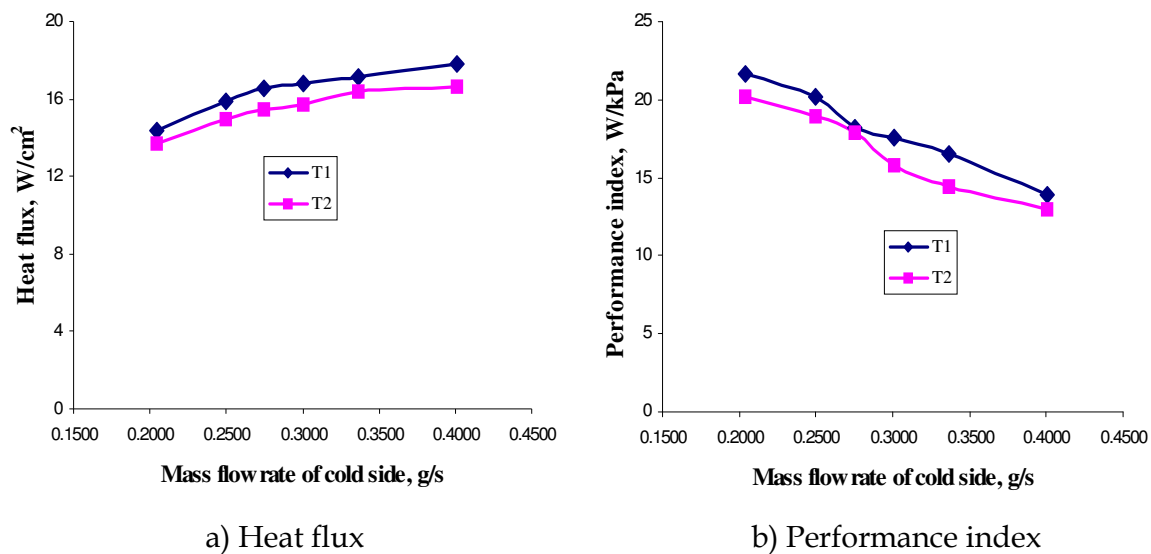


Fig. 21. Effects of the substrate thickness with a rising mass flow rate of cold side.

For the case of increasing the mass flow rate of the cold side (Case 2 was developed to study the effects of substrate thickness at various mass flow rates of the cold side), the heat fluxes of the heat exchangers increase with rising mass flow rate of the cold side, as shown in Fig. 21. Fig. 21 shows the effects of the substrate thickness with rising mass flow rate of the cold side. For this case, the heat flux obtained from T1 is also higher than that obtained from T2, as shown in Fig. 21a. When the mass flow rate of the cold side increases, the pressure drop of the cold side also increases; when the mass flow rate of the cold side increases, the average temperature of the hot side decreases, resulting in an increase of the pressure drop of the hot side. Besides, it was observed from the experimental data that the pressure drops increase at a higher slope than those for the effectiveness. It is noted that the performance index decreases with the rising mass flow rate of the cold side, as shown in Fig. 21b; however, the performance index obtained from the T1 is higher than that obtained from T2.

The effects of cross-sectional areas

For the evaluation of the effects of cross-sectional areas on the fluid and heat transfer of the microchannel heat exchangers, two cases were investigated: (1) Case 1 for the study of the effects of cross-sectional area for the heat exchanger at various inlet temperatures of the hot side and (2) Case 2 for the study of the effects of cross-sectional area for the heat exchanger at various mass flow rates of the cold side. Two microchannel heat exchangers T1 and T3 are tested for the effects of magnitude of cross-sectional area on the behaviors of heat transfer and fluid flow. These two microchannel heat exchangers have the same physical configurations for their substrates, manifolds, and lengths of channels. However, only the cross-sectional areas of microchannels are different. The microchannels of T1 have a rectangular cross-section with width of 500 μm and depth of 300 μm ; the microchannel of T3, width of 500 μm and depth of 180 μm . These dimensions are listed in Table 2.

For Case 1, Fig. 22 shows the effects of the cross-sectional areas on the behaviors of heat flux, effectiveness, pressure drop, and performance index for T1 and T3 with the inlet temperatures of the hot side ranging from 45 to 70 $^{\circ}\text{C}$. The heat fluxes of the heat exchangers increase with

the inlet temperature of the hot side increasing, as shown in Fig. 6a. It is observed that the heat transfer rates obtained from T3 are higher than those obtained from T1, leading to the fact that heat fluxes obtained from T3 are higher than those obtained from T1. The results obtained from the present study are in good agreement with those obtained from [37]. Foli et al. [37] indicated that under the constant mass flow rate condition, the higher the heat flux, the lower the aspect ratio (defined as the ratio of the microchannel height to its width). Under the same condition, the mass flow rates are fixed for two cases T1 and T3 used in this study. The conductive thermal resistance of T1 was found to be lower than that of T3. However, the convective thermal resistance of T1 was found to be higher than that of T3. The heat fluxes obtained from Fig. 22a show that the effect of the convective thermal resistance on the overall thermal resistance (appeared in Eqs. (5) and (6)) of the microchannel heat exchangers is more significantly than that of the conductive thermal resistance.

The effectiveness obtained from T3 is higher than that obtained from T1, as shown in Fig. 22b. However, because that the hydraulic diameter of channel in T3 is smaller than that of channel in T1, this results in the velocity in the channel of T3 to be higher than that of T1, leading to a higher pressure drop in T3 than that in T1, as shown in Fig. 22c. It was found that the pressure drop of T3 is 2 times higher than that of T1, while the effectiveness of T3 is 1.04 times higher than that of T1. As a result, the performance index (defined as the ratio of the heat transfer rate to the pressure drop in the heat exchanger) obtained from T1 is higher than that obtained from T3, as shown in Fig. 22d.

For Case 2, Fig. 23 shows the effects of the cross-sectional area on the behaviors of heat flux and performance index for T1 and T3 with the mass flow rates of the cold side ranging from 0.2135 to 0.401 g/s. It was found that the heat fluxes of T3 are higher than those of T1, as shown in Fig. 23a. For microchannel heat exchanger T3, a heat flux of 18.7 W/cm² (or overall average heat transfer coefficient of 8,500 W/m²K) was achieved for water from the hot side having a fixed inlet temperature of 70 °C and a fixed mass flow rate of 0.2308 g/s and for water from the cold side having a fixed inlet temperature of 22.5 °C and a mass flow rate of 0.401 g/s. It was also found that the pressure drop of T3 is higher than that of T1; the curve of the pressure drop is at a higher slope than that of the heat flux; as a result, the performance index of T1 is higher than that of T3, as shown in Fig. 23b.

From Figs. 20-23 obtained in this study, it indicates that for the microchannel heat exchangers being investigated, the effect of the hydraulic diameter on the performance index is more pronounced than that of the substrate thickness. In addition, it demonstrates that the lower the hydraulic diameter, the higher the heat flux and the pressure drop.

The effects of inlet/outlet location

Again, in Dang [3] and Dang and Teng [25], two cases were investigated: (1) Case 1 for the study of the effects of inlet/out location for the heat exchanger at various inlet temperatures of the hot side and (2) Case 2 for the study of the effects of inlet/out location for the heat exchanger at various mass flow rates of the cold side. The inlet/outlet locations affect significantly the behaviors of heat transfer and fluid flow of the microchannel heat exchangers. The two microchannel heat exchangers T2 and T4 were tested for this case. These two heat exchangers have the same dimensions of the channel and manifold; however, as shown in Fig. 3, the configuration of manifold together with the channel for T2 is the S-type and that for T4 is the I-type. Parameters of the heat exchangers are listed in more detail in Table 2.

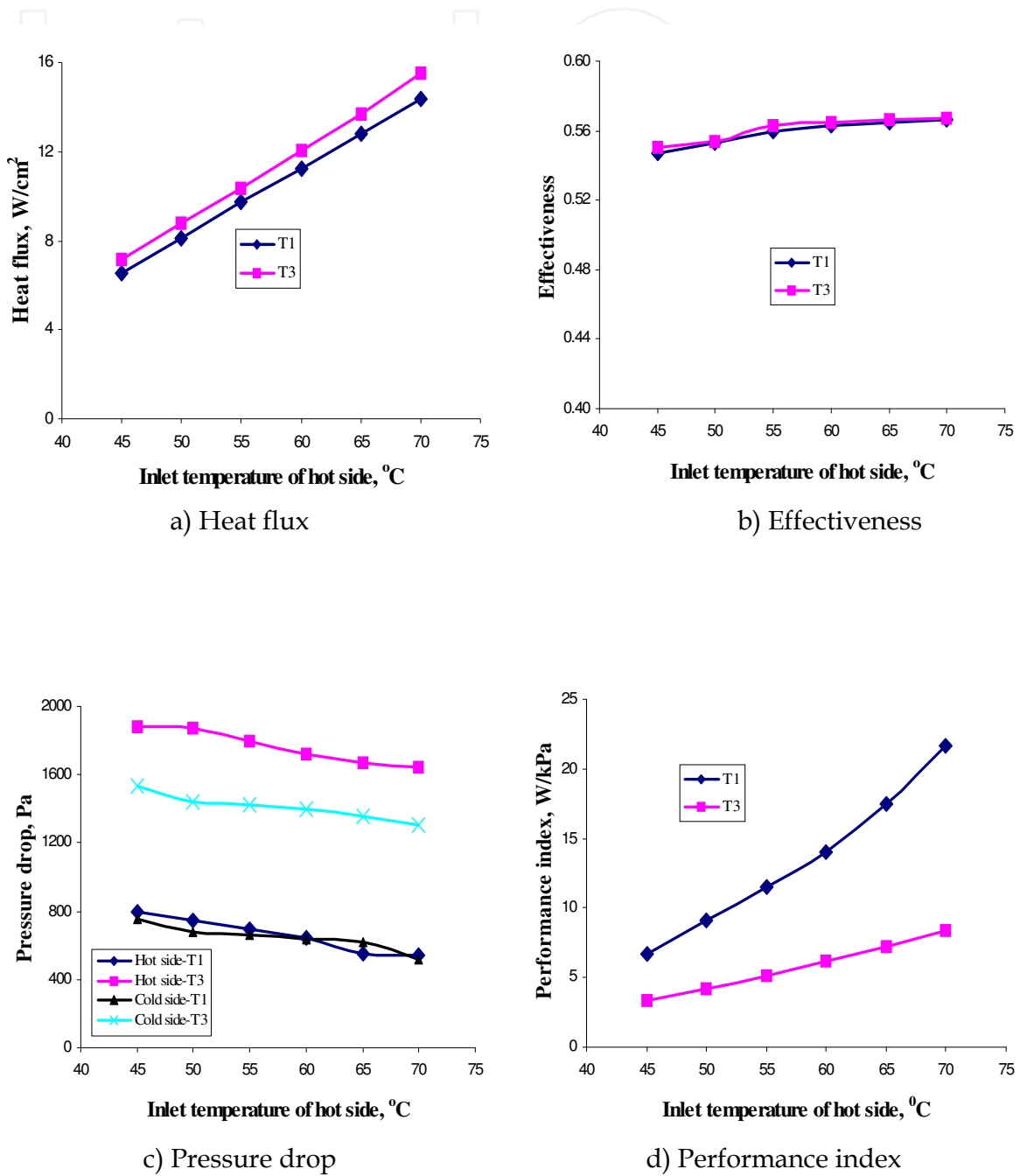


Fig. 22. Effects of the cross-sectional area with a rising inlet temperature of hot side.

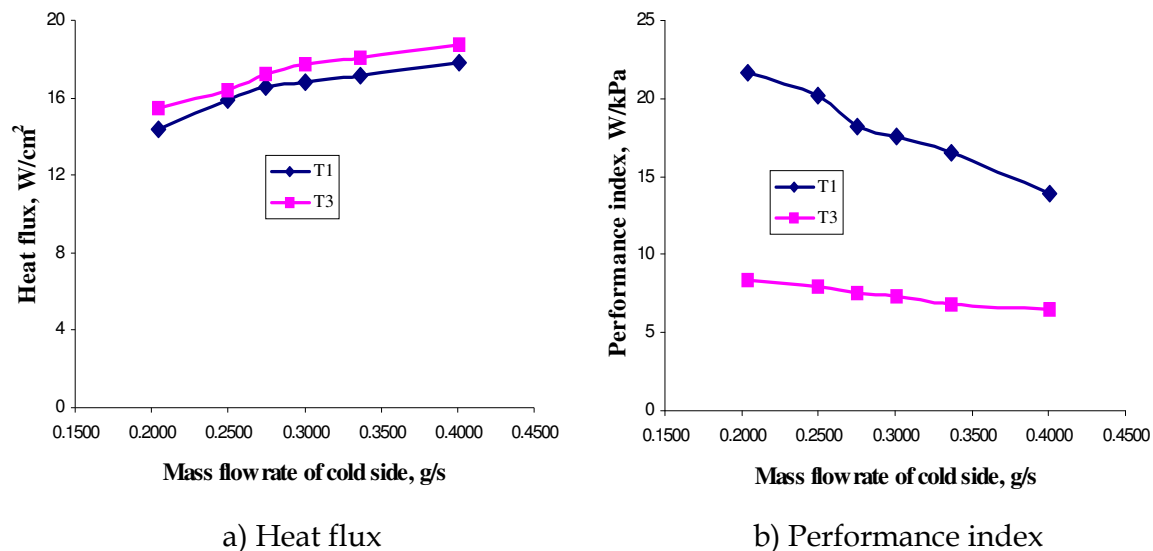


Fig. 23. Effects of the cross-sectional area with a rising mass flow rate of cold side.

For Case 1, Fig. 24 shows the effects of the inlet/outlet location on the behaviors of heat flux, effectiveness, pressure drop, and performance index for heat exchangers T2 and T4 with the inlet temperatures of the hot side ranging from 45 to 70 °C. In these two heat exchangers, the effects of maldistribution by the manifolds are important for heat transfer and pressure drop. The distance of flow path for the fluid moving from the entrance to the exit for the S-type microchannel heat exchanger is longer than that for the I-type, leading to the fact that the heat flux of T2 is higher than that of T4, as shown in Fig. 24a; as a result, the effectiveness of T2 is also higher than that of T4, as shown in Fig. 24b. However, it is also due to the fact that the distance the fluid moves from the entrance to the exit for the S-type is longer than that obtained with the I-type, so the pressure drop obtained from T2 is higher than that obtained from T4 for the same mass flow rate through the two heat exchangers being investigated, as shown in Fig. 24c. Fig. 24d shows the performance index of the heat exchangers as a function of the inlet temperature of the hot side. The performance index obtained from T4 is higher than that obtained from T2.

For Case 2, Fig. 25 shows the effects of the cross-sectional area on the behaviors of heat flux and performance index for the heat exchangers T2 and T4 with the mass flow rates of the cold side ranging from 0.2135 to 0.401 g/s. It was found that the heat fluxes obtained from T2 are higher than those from T4, as shown in Fig. 25a. However, when the mass flow rates of the cold side increase, the pressure drops increase also, leading to the fact that the pressure drop of T4 is lower than that of T2. It was also found that the performance index of T4 is higher than T2, as shown in Fig. 25b.

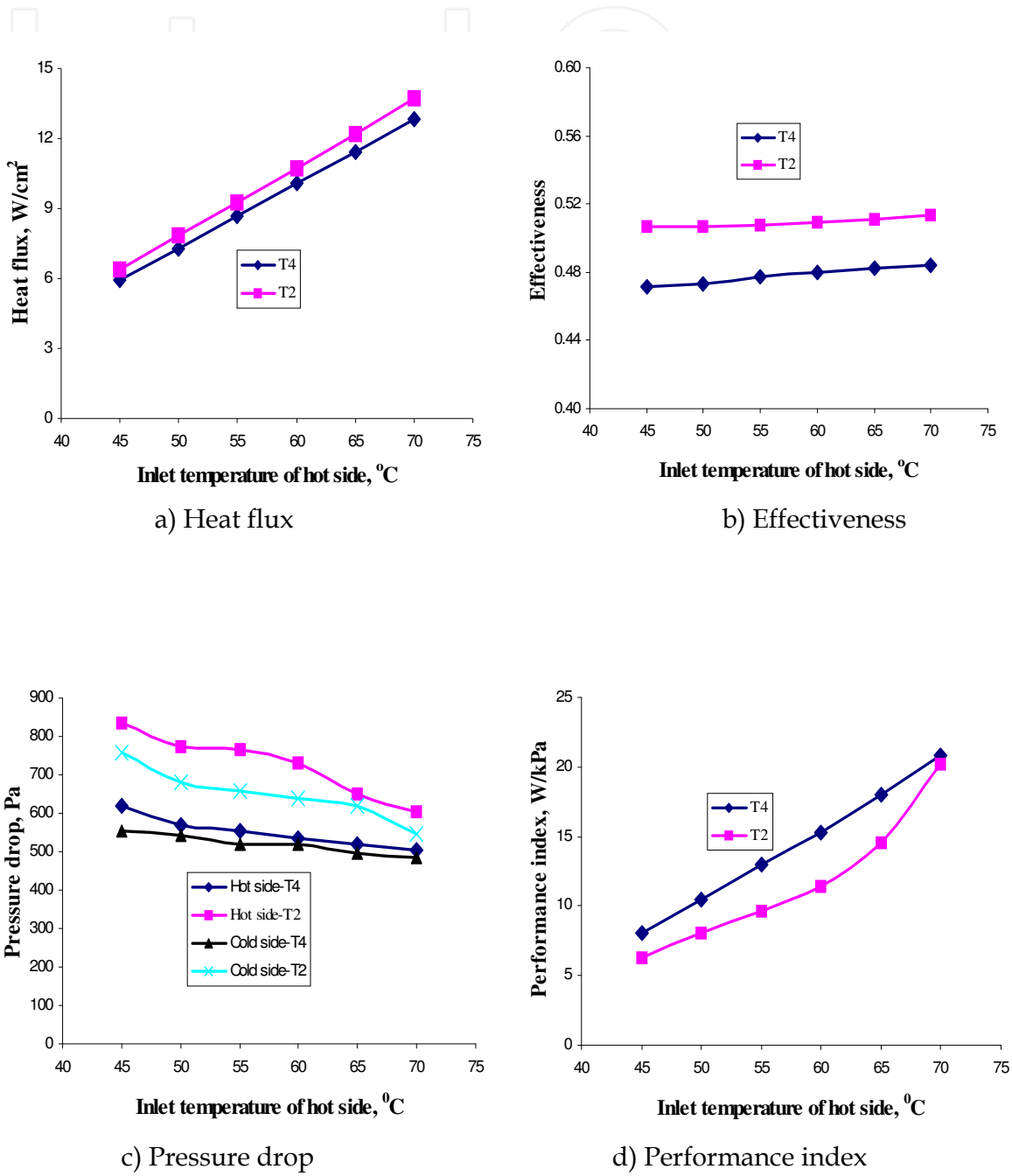


Fig. 24. Effects of the inlet/outlet location with a rising inlet temperature of hot side.

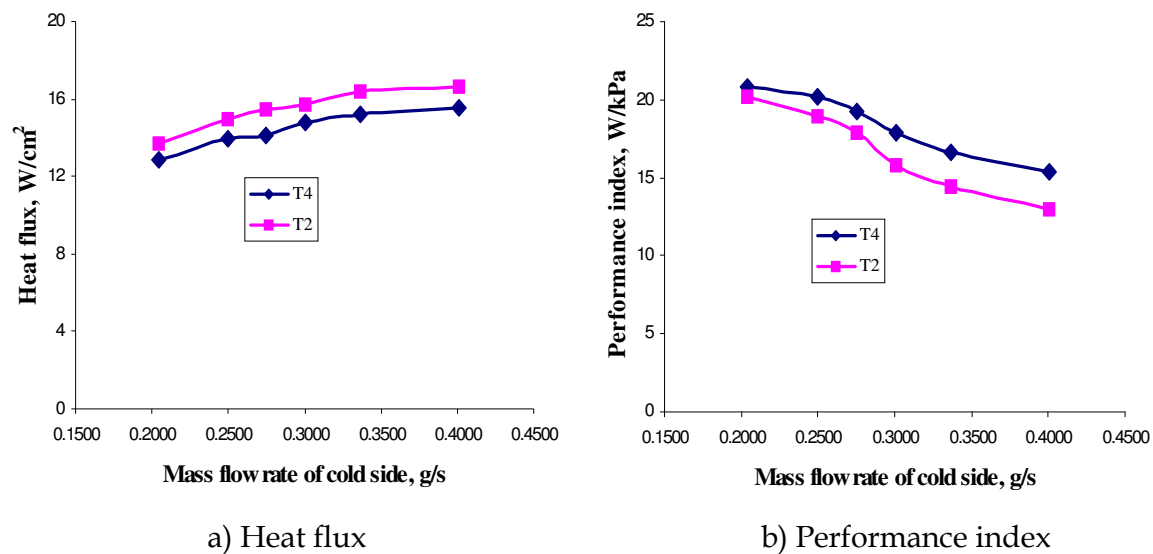


Fig. 25. Effects of the inlet/outlet location with a rising mass flow rate of cold side.

In summary, Figs. 20-25 indicate that the highest heat flux achievable for all cases studied is the microchannel heat exchanger T3. However, the performance index of T3 is lowest among all cases being investigated. It is observed that the heat flux and pressure drop obtained from the S-type manifold together with the channels are higher than that from the I-type. However, the performances indexes of both types of heat exchangers are essentially the same. For all cases studied, the microchannel heat exchanger T1 yields the highest performance index, with T4 being the second best. From the experimental data shown in Figs. 20-25, the overall average heat transfer coefficients of the heat exchangers with a value of $8,500 \text{ W}/(\text{m}^2\text{K})$ which was evaluated in this study are in good agreement with the overall heat transfer coefficient obtained in Kandlikar et al. [34] for microchannels with the same hydraulic diameter; however, the overall average heat transfer coefficient obtained from the present study is higher than that ($\sim 5,100 \text{ W}/(\text{m}^2\text{K})$) obtained in García-Hernando et al. [36] due to the difference in design.

4.4 Effects of gravity

An experimental study of the effects of gravity on the fluid in microchannel heat exchangers was carried out in the study to find out how does the gravity affect the behaviors of heat transfer and pressure drop for the microchannel heat exchangers? For the experimental system, the inlet temperature and the mass flow rate of the hot side were fixed at 70°C and 0.2308 g/s , respectively; at the cold side, the inlet temperature was fixed at 22.5°C and the mass flow rates were varying from 0.2135 to 0.401 g/s . In this study, influence of gravity was determined by two cases: one with horizontal channels, the other with vertical channels. For vertical channels, the hot water is flowing upward which is against the gravitational field, while the cold water is flowing downward which is in the same direction as the gravitational field [26,27]. Two microchannel heat exchangers T1 and T3 were tested: these two microchannel heat exchangers have the same physical configurations for their substrates, manifolds, and lengths of channels; only the cross-sectional areas of microchannels are different. The microchannels of T1 have a rectangular cross-section with width of $500 \mu\text{m}$ and depth of $300 \mu\text{m}$; the microchannel of T3, width of $500 \mu\text{m}$ and depth of $180 \mu\text{m}$. Parameters of the heat exchangers (T1 and T3) are listed in more detail in Table 2.

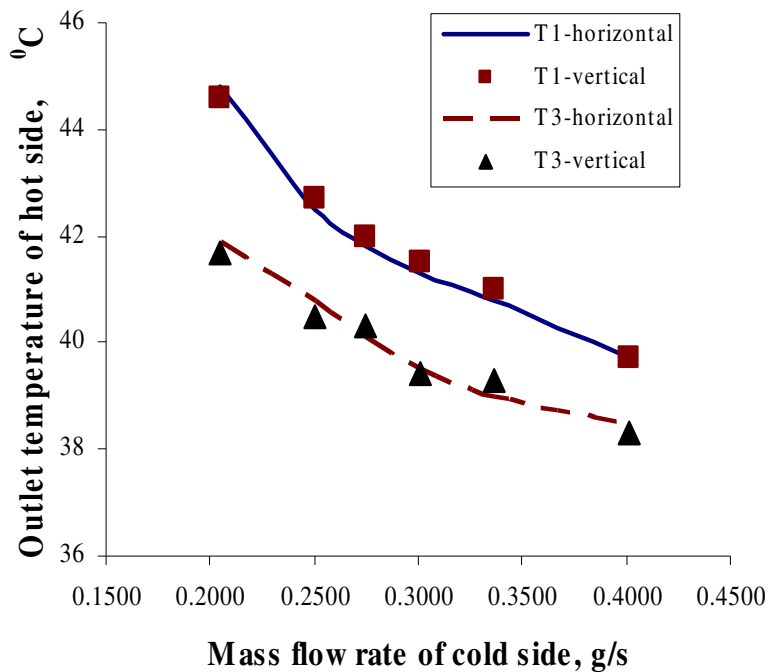


Fig. 26. Comparison of outlet temperatures of hot side.

Fig. 26 shows a comparison of at specified mass flow rate of the cold side the difference between outlet temperature of hot side obtained from a horizontal channel (either T1 or T3) and that from the vertical one (the corresponding T1 or T3) is negligibly small. A comparison of the outlet temperatures of cold side of two microchannel heat exchangers is shown in Fig. 27. The outlet temperatures (for both the hot and the cold sides) are functions of the mass flow rate of cold side; the outlet temperatures decrease as the mass flow rate of the cold side increases.

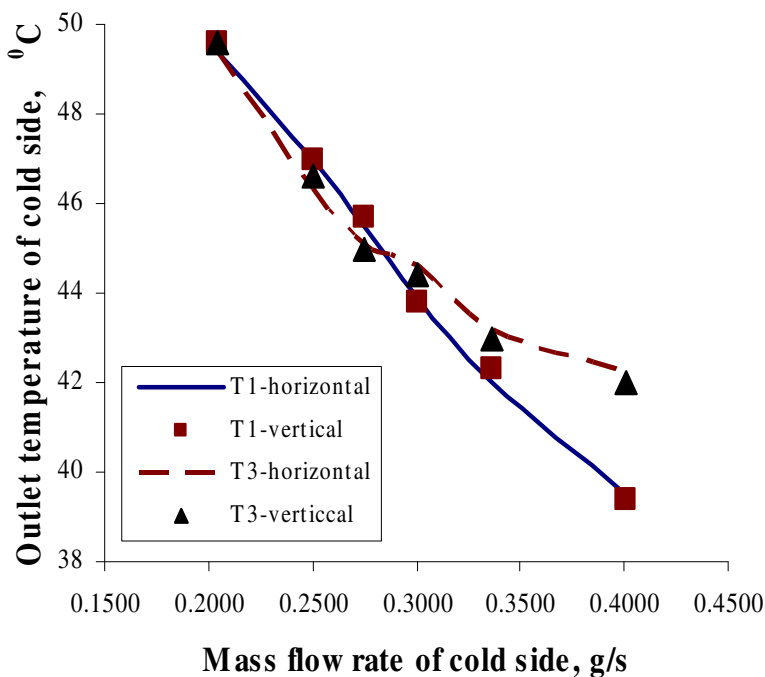


Fig. 27. Comparison of outlet temperatures of cold side.

The outlet temperatures of hot side obtained from T1 is higher than those obtained from T3; however, the outlet temperatures of cold side obtained from T1 is lower than those obtained from T3. As a result, the heat transfer rate obtained from T3 is higher than that obtained from T1, as shown in Fig. 28. The results obtained from the present study are in good agreement with those obtained from [37]. Foli et al. [37] indicated that under the constant mass flow rate condition, the higher the heat flux, the lower the aspect ratio (defined as the ratio of the microchannel height to its width).

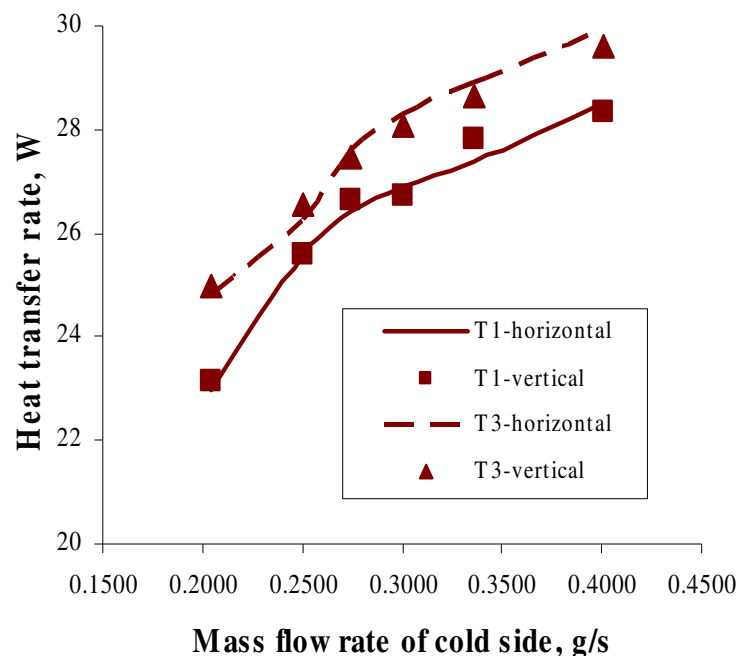


Fig. 28. Comparison of heat transfer rates.

It is shown from Fig. 28 that at specified mass flow rate of the cold side the difference between the heat transfer rate obtained from a horizontal channel (either T1 or T3) and that from the vertical one (the corresponding T1 or T3) is negligibly small. The heat transfer rate of the heat exchangers is a function of the mass flow rate of cold side: it increases from 24.8 to 29.92 W with the mass flow rate of cold side rising from 0.2043 to 0.401 g/s (for the heat exchanger T3).

Because that the hydraulic diameter of channel in T3 is smaller than that of channel in T1, this results in the velocity in the channel of T3 to be higher than that of T1, leading to a higher total pressure drop in T3 than that in T1, as shown in Fig. 29. Besides, the figure shows that the total pressure drop is a function of Reynolds number of cold side; the total pressure drop increases as rising the Re number of cold side.

Experimental results for effects of gravity on the behavior of pressure drop for the microchannel heat exchanger are also shown in Fig. 29. It is observed that the change of pressure drop between the two cases (horizontal channels and vertical channels) is negligibly small; the maximum change in pressure is 7.2% for a pressure drop from 1060 to 2044 Pa.

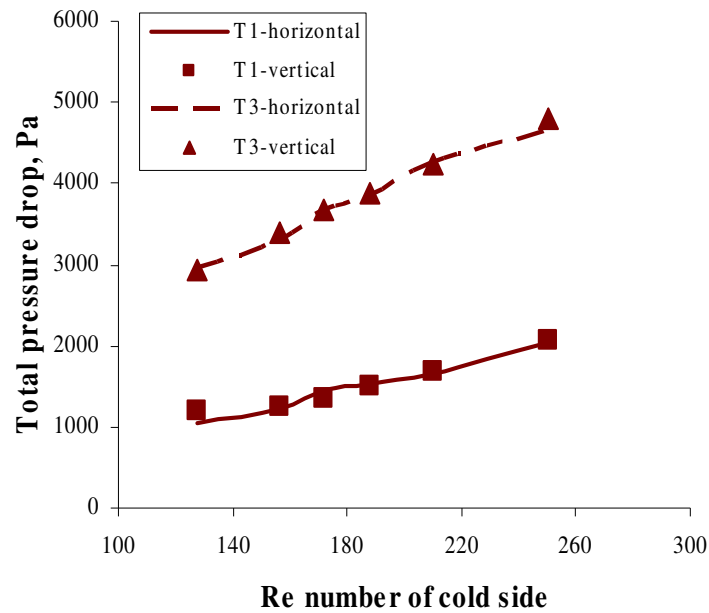


Fig. 29. Comparison of total pressure drops.

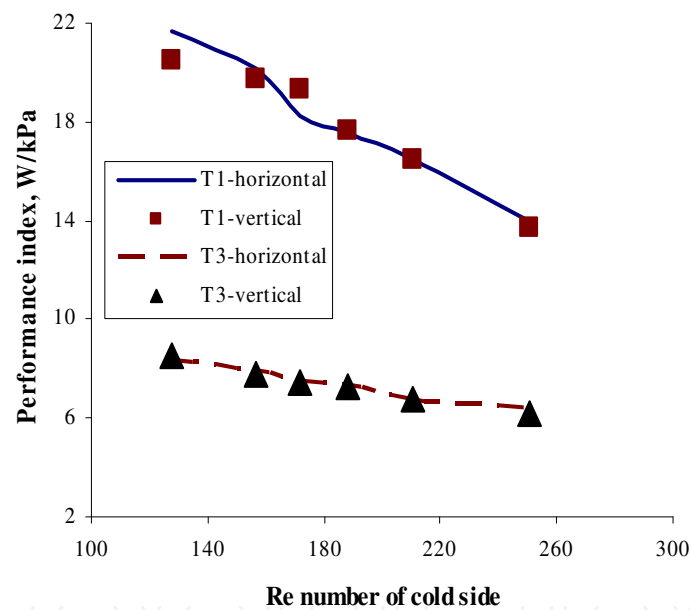


Fig. 30. Comparison of performance indices.

It was found that the pressure drop of T3 is 2 times higher than that of T1, while the heat transfer rate of T3 is 1.06 times higher than that of T1. As a result, the performance index (defined as the ratio of the heat transfer rate to the pressure drop in the heat exchanger) obtained from T1 is higher than that obtained from T3, as shown in Fig. 30. For heat exchanger T1, a performance index of 21.68 W/kPa was achieved for water from the hot side having an inlet temperature of 70 °C and a mass flow rate of 0.2308 g/s and for water from the cold side having an inlet temperature of 22.5 °C and mass flow rate of 0.2135 g/s. It is also observed that the change of performance between the two cases (horizontal channels and vertical channels) is negligibly small; the maximum change in performance is 5.5%, out of a performance index from 13.69 to 21.68 W/kPa.

In summary, it is concluded that for both heat transfer and pressure drop behaviors, the impact of gravity on the fluid flowing through the microchannel heat exchange can be ignored as indicated in [3,26,27,33,34].

5. Conclusion

In this study, for the cases with both inlet temperature and mass flow rate constant at the cold side of the device, the trends for the results obtained from the actual effectiveness method and those obtained from the effectiveness (ε -NTU) method are in the opposite directions as the mass flow rate of the hot side increases. However, for the cases with constant inlet temperature and mass flow rate at the hot side of the device, the trends for the results obtained from both methods for evaluating effectiveness are in the same directions.

With all cases done in the study, the performance index obtained from the counterflow is always higher than that obtained from the parallel-flow. As a result, the microchannel heat exchanger with counter-flow should be selected to use for every case (except few special cases).

In the study, it indicates that the substrate thickness affects negligibly the parameters associated with the heat transfer process of the heat exchangers with the substrate thicknesses of 1.2 and 2 mm. The effect of the hydraulic diameter (cross-sectional area) on the performance index is more pronounced than that of the substrate thickness. In addition, it demonstrates that the lower the hydraulic diameter, the higher the heat flux and the pressure drop. Regarding the effects of inlet/outlet locations, for two types (I-type and S-type) of the microchannel heat exchangers, the heat flux and pressure drop obtained from the S-type are higher than those from the I-type, even though the performance indexes of both heat exchangers are essentially the same.

The impact of gravity on the fluid flowing through the microchannel heat exchanger was found to be small, with the maximum difference between the results of horizontal and vertical channels being less than 8%. In addition, in this study, good agreements were achieved between the results obtained from the present study and the results obtained from the literatures.

In the study, good agreements were achieved for the behaviors of heat transfer and fluid flow between the results obtained from numerical simulations and those obtained from experimental data for fluid flowing in the counter-flow microchannel heat exchanger used, with the maximum percentage difference between the two results of less than 9%.

This chapter summarized the work performed and the results obtained both in the fluid flow and heat transfer done by TFAG over the last several years. The authors would like to express their deep appreciation for the financial supports obtained from National Science Council, the Republic of China in Taiwan (Grant Nos. NSC93-2212-E-033-012, NSC94-2212-E-033-017, NSC95-2212-E-033-066, NSC96-2212-E-033-039, NSC97-2212-E-033-050, NSC99-2212-E-033-025, and NSC 100-2221-E-033-065) and Chung Yuan Christian University (Grant No. CYCU-98-CR-ME).

6. Nomenclature

| | |
|-------|-----------------------------|
| A_c | cross-sectional area, m^2 |
| D_h | hydraulic diameter, m |
| f | friction factor |

| | |
|-----------------|---|
| h | heat transfer coefficient, W/m ² K |
| k | overall heat transfer coefficient, W/m ² K |
| K _r | thermal conductivity ratio |
| K _v | volumetric heat transfer coefficient, W/m ³ K |
| L | length of channel, m |
| | distance from the nozzle to the breakdown point of the jet, m |
| m | mass flow rate, kg/s |
| n | number of tubes |
| NTU | Number of Transfer Unit |
| Nu | Nusselt number |
| \overline{Nu} | average Nusselt number |
| p | pressure, Pa |
| P | wetted perimeter, m |
| Q | heat transfer rate, W |
| q | heat flux, W/m ² |
| R | thermal resistance, m ² K/W |
| Re | Reynolds number |
| T | temperature, K |
| T _d | mean temperature, K |
| V | volume flow rate, m ³ /s |
| Z | nozzle-to-wall distance, m |

Greek symbols

| | |
|----|--------------------------------------|
| μ | dynamic viscosity, Ns/m ² |
| ρ | density, kg/m ³ |
| λ | thermal conductivity, W/mK |
| ω | velocity, m/s |
| ε | effectiveness |
| ξ | performance index, W/kPa |
| φ | liquid fill ratio |
| ΔT | different temperature, K |
| Δp | pressure drop, Pa |

7. References

- [1] W.J. Bowman and D. Maynes (2001): A review of micro-heat exchanger flow physics, fabrication methods and application, Proceedings of ASME IMECE 2001, New York, USA, Nov 11-16, HTD-24280, pp. 385-407
- [2] G.L. Morini (2004): Single-phase convective heat transfer in microchannels: a review of experimental results, *Int. J. of Thermal Sciences*, Vol. 43, 631-651
- [3] T.T. Dang (2010): A study on the heat transfer and fluid flow phenomena of microchannel heat exchanger, Ph.D. thesis, Chung Yuan Christian University, Chung-Li, Taiwan
- [4] T.T. Dang, J.T. Teng, and J.C. Chu, Pressure drop and heat transfer characteristics of microchannel heat exchangers: A review of numerical simulation and experimental data (Accepted for Publication), *International Journal of Microscale and Nanoscale Thermal and Fluid Transport Phenomena*, 2011

- [5] J.J. Brandner, L. Bohn, T. Henning, U. Schygulla and K. Schubert (2006): Microstructure heat exchanger applications in laboratory and industry, Proceedings of ICNMM2006, Limerick, Ireland, June 19-21, ICNMM2006-96017, pp. 1233-1243
- [6] S.W. Kang and S.C. Tseng (2007): Analysis of effectiveness and pressure drop in micro cross-flow heat exchanger, *Applied Thermal Engineering*, Vol. 27, 877-885
- [7] T. Henning, J.J. Brandner and K. Schubert (2004): Characterisation of electrically powered micro-heat exchangers, *Chemical Engineering Journal*, Vol. 101, 339-345
- [8] J.J. Brandner, E. Anurjew, L. Bohn, E. Hansjosten, T. Henning, U. Schygulla, A. Wenka, and K. Schubert (2006): Concepts and realization of microstructure heat exchangers for enhanced heat transfer, *Experimental Thermal and Fluid Science*, Vol. 30, 801-809
- [9] E. R. Delsman, M. H. J. M. de Croon, G. J. Kramer, P. D. Cobden, Ch. Hofmann, V. Cominos and J. C. Schouten (2004): Experiments and modelling of an integrated preferential oxidation-heat exchanger microdevice, *Chemical Engineering Journal*, Vol. 101, 123-131
- [10] E.R. Delsman, M.H.J.M.D Croon, A. Pierik, G.J. Kramer, P.D. Cobden, Ch. Hofmann, V. Cominos and J.C. Schouten (2004): Design and operation of a preferential oxidation microdevice for a portable fuel processor, *Chemical Engineering Science*, Vol. 59, 4795-4802
- [11] C. H. Shen and C. Gau (2004): Heat exchanger fabrication with arrays of sensors and heaters with its micro-scale impingement cooling process analysis and measurements, *Sensors and Actuators A: Physical*, Vol. 114, 154-162
- [12] C. Gillot, A. Bricard and C. Schaeffer (2000): Single and two-phase heat exchangers for power electronic components, *Int. J. of Thermal Sciences*, Vol. 39, 826-832
- [13] B. Alm, U. Imke, R. Knitter, U. chygulla and S. Zimmermann (2008): Testing and simulation of ceramic micro heat exchangers, *Chemical Engineering Journal*, Vol. 135, S179-S184
- [14] B. Hallmark, C.H. Hornung, D. Broady, C. Price-Kuehne and M.R. Mackley (2008): The application of plastic microcapillary films for fast transient micro-heat exchange, *Int. J. Heat Mass Transfer*, Vol. 51, 5344-5358
- [15] P.X. Jiang, M.H. Fan, G.S. Si and Z.P. Ren (2001): Thermal-hydraulic performance of small scale micro-channel and porous-media heat-exchangers, *Int. J. Heat Mass Transfer*, Vol. 44, 1039-1051
- [16] Schulz, G.N. Akapiev, V.V. Shirikova, H. Rösler and S.N. Dmitriev (2005): A new method of fabrication of heat transfer surfaces with micro-structured profile, *Nuclear Instruments and Methods in Physics Research Section B: Beam Interactions with Materials and Atoms*, Vol. 236, 254-258
- [17] H. Lee, Y. Jeong, J. Shin, J. Baek, M. Kang and K. Chun (2004): Package embedded heat exchanger for stacked multi-chip module, *Sensors and Actuators A: Physical*, Vol. 114, 204-211
- [18] X. Wei (2004): Stacked microchannel heat sinks for liquid cooling of microelectronics devices, Ph.D. thesis, Academic Faculty, Georgia Institute of Technology
- [19] M.I. Hasan, A.A. Rageb, M. Yaghoubi, and H. Homayoni (2009): Influence of channel geometry on the performance of a counter flow microchannel heat exchanger, *Int. J. Thermal Sciences*, Vol. 48, 1607-1618
- [20] T.A. Ameel, R.O. Warrington, R.S. Wegeng and M.K. Drost (1997): Miniaturization technologies applied to energy systems, *Energy Conversion and Management*, Vol. 38, 969-982
- [21] T.T. Dang, Y.J. Chang and J.T. Teng (2009): A study on the simulations of a trapezoidal shaped micro heat exchanger, *Journal of Advanced Engineering*, Vol. 4, 397-402

- [22] T.T. Dang, J.T. Teng and J.C. Chu (2010): Effect of flow arrangement on the heat transfer behaviors of a microchannel heat exchanger, Proceedings of the International MultiConference of Engineers and Computer Scientists 2010 (IMECS2010), Hongkong, pp. 2209-2214 (Best student paper award)
- [23] T.T. Dang, J.T. Teng and J.C. Chu (2010): Effect of flow arrangement on the heat transfer behaviors of a microchannel heat exchanger, Lecture Notes in Engineering and Computer Science, Vol. 2182, 2209-2214
- [24] T.T. Dang and J.T. Teng (2010): Numerical and experimental studies of the impact of flow arrangement on the behavior of heat transfer of a microchannel heat exchanger, *IAENG International Journal of Applied Mathematics*, Vol. 40, 207-213
- [25] T.T. Dang and J.T. Teng (2010): Influence of flow arrangement on the performance for an aluminium microchannel heat exchanger, *IAENG Transactions on Engineering Technologies Volume 5, the American Institute of Physics (AIP)*, Vol. 1285, 576-590
- [26] T. Dang, J.T. Teng, and J.C. Chu (2010): A study on the simulation and experiment of a microchannel counter-flow heat exchanger, *Applied Thermal Engineering*, Vol. 30, 2163-2172
- [27] T.T. Dang, J.T. Teng, and J.C. Chu, Influence of Gravity on the Performance Index of Microchannel Heat Exchangers – Experimental Investigations, World Congress on Engineering (WCE 2011), London, U.K., pp. 2094-2099
- [28] T.T. Dang and J.T. Teng (2010): Effect of the substrate thickness of counter-flow microchannel heat exchanger on the heat transfer behaviors, Proceedings of the International Symposium on Computer, Communication, Control and Automation 2010 (3CA2010), Taiwan, pp. 17-20
- [29] T. Dang and J.T. Teng (2011): The effects of configurations on the performance of microchannel counter-flow heat exchangers-An experimental study, *Applied Thermal Engineering*, Vol. 31, 3946-3955
- [30] T.T. Dang and J.T. Teng (2011): Comparison on the heat transfer and pressure drop of the microchannel and minichannel heat exchangers, *Heat and Mass Transfer*, Vol. 47, 1311-1322
- [31] T.T. Dang and J.T. Teng (2010): Numerical simulation of a microchannel heat exchanger using steady-state and time-dependent solvers, ASME 2010 International Mechanical Engineering Congress & Exposition (IMECE2010), Vancouver, Canada, pp. 1-10
- [32] COMSOL Multiphysics version 3.5 – Documentation, 2008
- [33] L.M. Jiji, Heat Convection, Second edition, Springer, Verlag Berlin Heidelberg, 2009
- [34] S.G. Kandlikar, S. Garimella, D. Li, S. Colin, and M.R. King, Heat Transfer and Fluid Flow in Minichannels and Microchannels, Elsevier Pte Ltd, Singapore, 2006.
- [35] J.P. Holman, Experimental methods for engineers, McGraw-Hill, New York, 1984
- [36] N. García-Hernando, A. Acosta-Iborra, U. Ruiz-Rivas and M. Izquierdo, Experimental investigation of fluid flow and heat transfer in a single-phase liquid flow micro-heat exchanger, *International Journal of Heat and Mass Transfer* 52 (23-24) (2009) 5433-5446
- [37] K. Foli, T. Okabe, M. Olhofer, Y. Jin, and B. Sendhoff, Optimization of micro heat exchanger: CFD, analytical approach and multi-objective evolutionary algorithms, *International Journal of Heat and Mass Transfer* 49 (5-6) (2006) 1090-1099.



Heat Exchangers - Basics Design Applications

Edited by Dr. Jovan Mitrovic

ISBN 978-953-51-0278-6

Hard cover, 586 pages

Publisher InTech

Published online 09, March, 2012

Published in print edition March, 2012

Selecting and bringing together matter provided by specialists, this project offers comprehensive information on particular cases of heat exchangers. The selection was guided by actual and future demands of applied research and industry, mainly focusing on the efficient use and conversion energy in changing environment. Beside the questions of thermodynamic basics, the book addresses several important issues, such as conceptions, design, operations, fouling and cleaning of heat exchangers. It includes also storage of thermal energy and geothermal energy use, directly or by application of heat pumps. The contributions are thematically grouped in sections and the content of each section is introduced by summarising the main objectives of the encompassed chapters. The book is not necessarily intended to be an elementary source of the knowledge in the area it covers, but rather a mentor while pursuing detailed solutions of specific technical problems which face engineers and technicians engaged in research and development in the fields of heat transfer and heat exchangers.

How to reference

In order to correctly reference this scholarly work, feel free to copy and paste the following:

Thanhtrung Dang, Jyh-tong Teng, Jiann-cherng Chu, Tingting Xu, Suyi Huang, Shiping Jin and Jieqing Zheng (2012). Single-Phase Heat Transfer and Fluid Flow Phenomena of Microchannel Heat Exchangers, Heat Exchangers - Basics Design Applications, Dr. Jovan Mitrovic (Ed.), ISBN: 978-953-51-0278-6, InTech, Available from: <http://www.intechopen.com/books/heat-exchangers-basics-design-applications/single-phase-heat-transfer-and-fluid-flow-phenomena-of-microchannel-heat-exchangers>

INTECH
open science | open minds

InTech Europe

University Campus STeP Ri
Slavka Krautzeka 83/A
51000 Rijeka, Croatia
Phone: +385 (51) 770 447
Fax: +385 (51) 686 166
www.intechopen.com

InTech China

Unit 405, Office Block, Hotel Equatorial Shanghai
No.65, Yan An Road (West), Shanghai, 200040, China
中国上海市延安西路65号上海国际贵都大饭店办公楼405单元
Phone: +86-21-62489820
Fax: +86-21-62489821

© 2012 The Author(s). Licensee IntechOpen. This is an open access article distributed under the terms of the [Creative Commons Attribution 3.0 License](#), which permits unrestricted use, distribution, and reproduction in any medium, provided the original work is properly cited.

IntechOpen

IntechOpen